J. Fluid Mech. (2004), *vol.* 507, *pp.* 1–42.
DOI: 10.1017/S0022112004007888 Printed in the United Kingdom

Structure of unsteady stably stratified turbulence with mean shear

By H. HANAZAKI[1]† AND J. C. R. HUNT[2,3]

[1]Institute of Fluid Science, Tohoku University, 2-1-1 Katahira, Aoba-ku, Sendai 980-8577, Japan

[2]Departments of Space and Climate Physics and Geological Sciences, University College London, Gower Street, London WC1E 6BT, UK

[3]J. M. Burgers Centre, Delft University of Technology, Delft, The Netherlands

(Received 14 February 2002 and in revised form 14 November 2003)

The statistics of unsteady turbulence with uniform stratification N (Brunt–Väisälä frequency) and shear $\alpha(=\mathrm{d}U_1/\mathrm{d}x_3)$ are analysed over the entire time range $(0<\alpha t<\infty)$ using rapid distortion theory (RDT) over a wide range of Richardson number $Ri(=N^2/\alpha^2)$, and initial conditions. The solutions are found to be described by the Legendre functions of complex degree with pure-imaginary argument and are compared with previously published results of both direct numerical simulations (DNS) and experiments. In the initial stage of development many of the characteristics are similar to those in stratified flow with no shear, since the turbulence is determined by Nt at the leading order, and the effects of vertical shear α generally appear at higher order. It is shown how in developing turbulence for $Ri>0$ and $Ri>0.25$ respectively, oscillatory momentum and positive and negative density fluxes develop. Above a critical value of $Ri_{crit}(\sim 0.3)$, their average values are persistently countergradient. This structural change in the turbulence is the primary mechanism whereby stable stratification reduces the fluxes and the production of variances. It is quite universal and differs from the energy and stability mechanisms of Richardson (1926) and Taylor (1931). The long-time asymptotics of the energy ratio $ER(=PE/VKE)$ of the potential energy to the vertical kinetic energy generally decreases with $Ri(\geqslant 0.25)$, reaching the smallest value of 3/2 when there is no shear $(Ri\to\infty)$. For strong mean shear $(Ri<0.25)$, RDT significantly overestimates ER since (as in unstratified shear flow) it underestimates the vertical kinetic energy VKE. The RDT results show that the asymptotic values of the energy ratio ER and the normalized vertical density flux are independent of the initial value of ER, in agreement with DNS. This independence of the initial condition occurs because the ratios of the contributions from the initial values PE_0 and KE_0 are the same for PE and VKE and can be explained by the linear processes. Stable stratification generates buoyancy oscillations in the direction of the energy propagation of the internal gravity wave and suppresses the generation of turbulence by mean shear. Because the shear distorts the wavenumber fluctuations, the low-wavenumber spectrum of the vertical kinetic energy has the general form $E_{33}(k)\propto(\alpha tk)^{-1}$, where $(L_X\alpha t)^{-1}\ll k\ll L_X^{-1}$ (L_X: integral scale). The viscous decay is controlled by the shear, so that the components of larger streamwise wavenumber k_1 decay faster. Then, combined with the spectrum distortion by the shear, the energy and the flux are increasingly dominated by the small-k_1 components as time elapses. They oscillate at the buoyancy period π/N because even in a shear flow the components as $k_1\to 0$ are weakly affected by the shear. The effects of stratification

† Present address: Department of Mechanical Engineering, Kyoto University, Yoshida-Honmachi, Sakyo-ku, Kyoto 606-8501, Japan.

N and shear α at small scales are to reduce both VKE and PE. Even for the same Ri, larger N and α reduce the high-wavenumber components of VKE and PE. This supports the applicability of the linear assumption for large N and α. At large scales, the stratification and shear effects oppose each other, i.e. both VKE and PE decrease due to the stratification but they increase due to the shear. We conclude that certain of these unsteady results can be applied directly to estimate the properties of sheared turbulence in a statistically steady state, but others can only be applied qualitatively.

1. Introduction

Turbulence is not a universal state of nature, but there are similar forms of eddy motion, and mixing processes with similar statistical properties for a variety of turbulent flows within a particular 'type'. These 'types' are determined by the form of the large-scale motion or forcing or initial/boundary conditions (e.g. shear flows, buoyant convection etc.) Studying both the qualitative features and the statistics is necessary to predict and understand the effects of turbulence on other processes such as heat and mass transfer (Holmes, Lumley & Berkooz 1996; Hunt *et al.* 2001).

Stably stratified turbulent flows with weak mean shear are members of one important 'type', and research in the past 50 years has demonstrated how similar characteristic features of the eddy motion, and characteristic values of the dimensionless groups and other statistical relations are found in stably stratified shear flows whether in the atmosphere, ocean or engineering (e.g. Hunt, Kaimal & Gaynor 1985; Gargett 1986; Schumann 1996).

The aim of this paper is to build on previous laboratory, theoretical and numerical studies (e.g. water tank experiments by Komori *et al.* 1983 and Rohr *et al.* 1988, wind-tunnel experiments by Piccirillo & Van Atta 1997, direct numerical simulations (DNS) by Gerz, Schumann & Elghobashi 1989, Holt, Koseff & Ferziger 1992 and Jacobitz, Sarkar & Van Atta 1997, and large eddy simulation (LES) by Kaltenbach, Gerz & Schumann 1994) and explain how a number of these properties change as the mean shear varies, while the flow remains stably stratified. Although we focus on homogeneous flows with uniform gradients, such idealized flows describe many, but not all, features of stably stratified turbulence that occur in complex flows. There are certainly important exceptions such as where the turbulence is driven by wave motion generated some distance away. An intrinsic feature of spatially homogeneous turbulence is that it is unsteady, even in the presence of mean shear. This is because the turbulence structure keeps changing so that the production of turbulent energy is not equal to its loss by dissipation and conversion to potential energy. Consequently (cf. Townsend 1976) one has to be cautious about the direct application of results from these idealized flows to steady inhomogeneous flows.

There are three major unsolved problems on turbulence in stratified shear flows.

(1) The first of the problems to be addressed is to quantify the mechanisms for the suppression of turbulence in shear flows ($\mathrm{d}U_1/\mathrm{d}x_3 = \alpha$) by stable stratification, with buoyancy frequency $N = [(-g/\rho_0)\mathrm{d}\overline{\rho}/\mathrm{d}x_3]^{1/2}$. The fact that the mean velocity profile is exponentially unstable/stable to small disturbances when the Richardson number $Ri(= N^2/\alpha^2)$ is less/greater than a critical value Ri_{cri} (typically 0.25), has been proposed as the main suppression mechanism in such flows (Taylor 1931; Miles 1961). There are two objections to this explanation. First, experiments show that turbulence persists, even if intermittently, above this value. Secondly, this stability argument does

not apply to homogeneous shear flows where small disturbances grow algebraically, and not exponentially.

For both these types of flows Richardson's (1926) energy arguments can be applied, namely that as Ri increases the vertical velocity fluctuations are damped. This is only a partial explanation for the suppression mechanism because it implies that there should be a gradual decay of turbulence as Ri increases above 1.0, inconsistent with the observation of quite a sudden suppression as Ri increased above 0.25. Similarly most statistical turbulence models predict the sudden suppression of turbulence because they are based on approximate relations between turbulent energy and Reynolds stresses (e.g. Craft, Ince & Launder 1996).

Previous studies have shown that the shear stress $-\overline{u_1 u_3}$ and thence the production of turbulence by shear ($-\overline{u_1 u_3}\mathrm{d}U/\mathrm{d}x_3$) is in fact reduced by changes in the phase between vertical and horizontal velocity fluctuations as the particles' vertical motion tends to become more oscillatory in stable stratification (e.g. see Galmiche & Hunt 2002). To summarize, there remain uncertainties about the mechanisms in the different stages of the suppression process as Ri increases.

(2) The second problem concerns the large-scale vertical displacements Z of fluid particles that tend to be oscillatory on a time scale of order N^{-1} and are limited to a length scale l_B of order σ_w/N, where $\sigma_w = \overline{u_3^2}^{1/2}$ is the r.m.s. vertical velocity (a result of Lagrangian modelling by Csanady 1964, Pearson, Puttock & Hunt 1983, Kimura & Herring 1996, Kaneda 2000, Kaneda & Ishida 2000). Experiments at very high Reynolds numbers ($Re \sim \sigma_w L_X/\nu = 10^3$, where L_X is the integral scale (Britter *et al.* 1983) show that, as a result of fluid elements mixing with their surroundings, the variance of Z ($\overline{Z^2}$), after levelling out at time N^{-1}, increases very slowly on a time scale $\gamma^{-2}N^{-1}$, where $\gamma \ll 1$. Kimura & Herring's (1996) low Reynolds number DNS of rapidly decaying stratified turbulence show that $\gamma = 0$. The Lagrangian models show $\gamma = 0$ or $\gamma \neq 0$ depending on their parameterization of mixing. From Taylor (1921) it follows that the forms of the Lagrangian autocorrelation function and spectra must also be sensitive to the value of γ (Fernando & Hunt 1996). No quantitative model shows how at high Reynolds numbers γ tends to increase in the presence of shear.

These limited vertical displacements determine the level of r.m.s. fluctuation of density ρ and also of any passive scalar (such as pollutant concentration). Normalized on the mean density gradient, the magnitude of $\sigma_\rho = (\overline{\rho^2})^{1/2}$ can be interpreted physically in terms of a 'density' or Ellison length scale $l_\rho = \sigma_\rho/|\mathrm{d}\overline{\rho}/\mathrm{d}x_3|$. Experiments in sheared and unsheared stratified flows (e.g. Hunt *et al.* 1985; Monti *et al.* 2002) show that l_ρ is of the same order as l_B, i.e.

$$l_\rho/l_B = \xi_\rho \sim 1,$$

when the stratification is strong, $Fr = \sigma_w/NL_X \leqslant 1$, where Fr is the Froude number.

(3) Since the mass flux is caused by particles being displaced (i.e. macro mixing) and then exchanging matter with other particles (micro mixing), the reduction in the vertical displacement (Z) affects the mean density flux ($-\overline{\rho u_3}$) and the eddy diffusivity $\kappa_\rho = -\overline{\rho u_3}/(\mathrm{d}\overline{\rho}/\mathrm{d}x_3)$.

When normalized by l_B and σ_w, κ_ρ and the flux are determined by the dimensionless ratio $\mathscr{F}$, where $\mathscr{F} = \kappa_\rho/(\sigma_w l_B)$. In stable flows without shear $\mathscr{F}$ is found to be very small (~ 0.1), but in sheared flows the mixing is large (Hunt *et al.* 1985), as also occurs in unstratified flows (e.g. Sawford & Hunt 1986).

In unsteady developing stably stratified flows, the oscillation of the particle displacements causes $\mathscr{F}$ to be negative for an increasing proportion of the time, i.e.

there is a countergradient mass flux (e.g. Piccirillo & Van Atta 1997; Hunt, Stretch & Britter 1988). But as with the countergradient Reynolds stress, it is necessary to examine systematically how shear affects this change.

When there is no shear, the results of RDT (Hanazaki & Hunt 1996) have shown how the initial conditions determine the subsequent time development of the partition of energy between the potential energy and the kinetic energy. In addition, the change of sign in the vertical density flux with time, which leads to the so-called countergradient flux, could be explained by the simple linear oscillations due to buoyancy effects rather than by a new kind of nonlinear mixing processes. The changes in the spectra and cospectra derived by DNS and moderate Reynolds number laboratory experiments for unsteady developing flows could also be estimated by linear theory. However, for very high Reynolds number stably stratified flows, where buoyancy forces do not affect the smallest scales in the spectrum, the use of RDT requires a heuristic assumption about the time scale for each wavenumber range over which the linear processes are effective (Derbyshire & Hunt 1993).

In this study we extend the method to flow with mean shear. There are two time scales N^{-1} and α^{-1}, two internal length scales u_3'/N and u_3'/α (u_3' is the r.m.s. value of the vertical velocity) and an imposed length scale L_X. By assuming that $Fr = u_3'/(NL_X) \leqslant 1$ and $\alpha L_X/u_3' \geqslant 1$, the linear effects of stratification and mean shear dominate the dynamics of the energy-containing eddies for high Reynolds number turbulence and for the whole spectrum for low/moderate Reynolds number turbulence. Before starting this calculation we note (following Townsend 1976 and Kevlahan & Hunt 1997) that if certain velocity components are suppressed relative to others, nonlinear processes can feed energy to these components. So for these components the linear theory underestimates the results.

For the first time, the RDT equations for stably stratified shear flows have been solved analytically for arbitrary time. The results are consistent with the time development of the spectra and the fluxes which have been obtained by the short-time analytical approximations (some of which have been obtained previously). Numerical integrations of the solutions are used to derive the variances and spectra for moderate to long time developments over a wide range of Ri.

2. RDT equations

We consider a homogeneous turbulent flow stratified ($\mathrm{d}\overline{\rho}/\mathrm{d}x_3$) and sheared ($\alpha = \mathrm{d}U_1/\mathrm{d}x_3$) in the vertical ($x_3$) direction. The governing equations of rapid distortion theory (RDT) (Batchelor & Proudman 1954; Townsend 1976; Stretch 1986; Hunt *et al.* 1988) which describe the turbulence in the frame of reference moving with the mean shear flow are

$$\left(\frac{\mathrm{d}}{\mathrm{d}t} + \nu k^2\right)\hat{u}_i = \alpha \hat{u}_3 \left(\frac{2k_i k_1}{k^2} - \delta_{i1}\right) + \left(\frac{k_i k_3}{k^2} - \delta_{i3}\right)\hat{\rho}, \tag{2.1}$$

$$\left(\frac{\mathrm{d}}{\mathrm{d}t} + \kappa k^2\right)\hat{\rho} = N^2 \hat{u}_3, \tag{2.2}$$

where N is the Brunt–Väisälä frequency given by $N^2 = -(g/\rho_0)(\mathrm{d}\overline{\rho}/\mathrm{d}x_3)$, and $\hat{u}_i (i = 1, 2, 3)$ and $\hat{\rho}$ are defined by

$$u_i = \sum_{\boldsymbol{k}(t)} \hat{u}_i(\boldsymbol{k}(t), t) \mathrm{e}^{\mathrm{i}\boldsymbol{k}(t)\cdot\boldsymbol{x}}, \tag{2.3}$$

and

$$\frac{g}{\rho_0}\rho = \sum_{\boldsymbol{k}(t)} \hat{\rho}(\boldsymbol{k}(t), t)\mathrm{e}^{\mathrm{i}\boldsymbol{k}(t)\cdot\boldsymbol{x}}. \tag{2.4}$$

Here, ρ_0 is the reference density, ρ is the perturbation density, g is the acceleration due to gravity, ν is the viscosity coefficient and κ is the diffusion coefficient.

The wavenumber vector develops with time as

$$\frac{\mathrm{d}k_i}{\mathrm{d}t} = -\alpha k_1 \delta_{i3}, \tag{2.5}$$

which gives

$$\boldsymbol{k}(t) = (k_1, k_2, k_3) = (k_{10}, k_{20}, k_{30} - \alpha t k_{10}), \tag{2.6}$$

where $\boldsymbol{k}_0 = (k_{10}, k_{20}, k_{30})$ is the initial wavenumber.

In this study we use a spherical coordinate in the spectral space defined by

$$k_1 = k\sin\theta\cos\phi, \quad k_2 = k\sin\theta\sin\phi, \quad k_3 = k\cos\theta, \tag{2.7}$$

where $k = (k_1^2 + k_2^2 + k_3^2)^{1/2}$, $0 \leqslant \theta \leqslant \pi$, and $0 \leqslant \phi \leqslant 2\pi$. Then, the initial wavenumber vector satisfies

$$k_{10} = k_0\sin\theta_0\cos\phi_0, \quad k_{20} = k_0\sin\theta_0\sin\phi_0, \quad k_{30} = k_0\cos\theta_0, \tag{2.8}$$

with $k_0 = (k_{10}^2 + k_{20}^2 + k_{30}^2)^{1/2}$, and the distorted wavenumber at time t becomes

$$k_1(t) = k(t)\sin\theta(t)\cos\phi_0, \quad k_2(t) = k(t)\sin\theta(t)\sin\phi_0, \quad k_3(t) = k(t)\cos\theta(t). \tag{2.9}$$

Since only the k_3 component changes with time, θ changes with time, while $\phi(=\phi_0)$ and the horizontal wavenumber $k_H \equiv (k_1^2 + k_2^2)^{1/2} = (k_{10}^2 + k_{20}^2)^{1/2} = k\sin\theta$ are invariant with time.

It is important to note the conditions for which the RDT in stably stratified shear flow is valid. They are that the nonlinear term $(\boldsymbol{u}\cdot\nabla)\boldsymbol{u}$ ($\boldsymbol{u} = (u_1, u_2, u_3)$, $|\boldsymbol{u}| = O(u)$) in the Navier–Stokes equations is small compared to either the buoyancy term $g\rho/\rho_0$ (Derbyshire & Hunt 1993) or the mean shear term $u_3\mathrm{d}U/\mathrm{d}x_3 (= \alpha u_3)$. At the same time the term $(\boldsymbol{u}\cdot\nabla)\rho$ must be small compared to $u_3\,\mathrm{d}\overline{\rho}/\mathrm{d}x_3$ in the equation for the density.

Using the eddy size l and its characteristic velocity $u(l)$, the nonlinear term is expressed as

$$(\boldsymbol{u}\cdot\nabla)\boldsymbol{u} = O\left(\frac{u^2}{l}\right), \tag{2.10}$$

while the buoyancy term is

$$\frac{g}{\rho_0}\rho = O(uN^2t) \text{ (if } \alpha t \ll 1 \text{ and } Ri \leqslant O(1) \text{ (cf. § 3.3))}, \tag{2.11}$$

$$= O(uN)\left(\text{if } Nt \geqslant 1 \text{ and } Fr_l = \frac{u}{Nl} \ll 1\right), \tag{2.12}$$

where Fr_l is the 'eddy' Froude number. Then, the buoyancy advection term is estimated as

$$(\boldsymbol{u}\cdot\nabla)\rho = O\left(uNt\frac{\mathrm{d}\overline{\rho}}{\mathrm{d}x_3}\right), \tag{2.13}$$

$$= O\left(u\frac{u}{Nl}\frac{\mathrm{d}\overline{\rho}}{\mathrm{d}x_3}\right), \tag{2.14}$$

for these two conditions. Therefore, $Fr_l = u/Nl \ll 1$ is the necessary condition for $O((\boldsymbol{u}\cdot\nabla)\rho) < O(u_3 \mathrm{d}\overline{\rho}/\mathrm{d}x_3)$ independent of whether time t is small or large, and this also ensures that nonlinear terms are smaller than buoyancy term, i.e. $O((\boldsymbol{u}\cdot\nabla)\boldsymbol{u}) < O((g/\rho_0)\rho)$, so that the RDT approximations become valid.

The ratio of the nonlinear term to the mean shear term is given at all times by $1/Sh_l$, where the eddy shear number Sh_l is defined by $Sh_l = \alpha l/u$. Since the eddy shear number and the eddy Froude number are related by $1/Sh_l = Fr_l Ri^{1/2}$, for a fixed Richardson number ($Ri \leqslant O(1)$), small $1/Sh_l$ is ensured automatically when $Fr_l \ll 1$. Then, the condition $1/Sh_l \ll 1$ is of only secondary importance for the validity of RDT when the condition $Fr_l \ll 1$ is already satisfied. Therefore, the applicability conditions for RDT are essentially the same as for the stratified flow with no shear as given by Hanazaki & Hunt (1996).

At low and moderate Reynolds numbers as in laboratory experiments and DNS, the eddy Froude number $Fr_l = u/Nl \ll 1$ is of the same order as the Froude number defined by $Fr_0 = u_0/Nl_0$, where u_0 is the r.m.s. velocity and l_0 is the scale of the energy-containing eddy. Then the RDT equations (2.1) and (2.2) are valid for $Fr_0 \ll 1$. On the other hand, at high Re, RDT is not valid for the small scales of turbulence even if Fr_0 is small (cf. Hanazaki & Hunt 1996). We note that for small Richardson numbers ($Ri < 0.25$) when linear instability occurs, for certain flows with non-uniform shear (Miles 1961), the comparison between RDT and DNS results shows poorer agreement as will be shown in § 6. This is because the condition of $Fr_l \ll 1$ is violated over a wide wavenumber range in this more energetic turbulence.

RDT also becomes invalid at very large times when velocity fluctuations become approximately two-dimensional in the horizontal plane, i.e. when $Fr \to 0$. Two kinds of motions occur: the slow nonlinear horizontal motion with time scale $t \sim l/u$ ($\gg N^{-1}$ if $Fr \ll 1$) or the fast ($t \sim N^{-1}$) linear wave motion, each of which described by the horizontal two-dimensional Navier–Stokes equations for the 'vortex' mode or the internal wave equations for the 'wave' mode (Riley, Metcalfe & Weissman 1981; Riley & Lelong 2000). RDT describes the fast wave modes, while the slow vortex mode with strong nonlinearity are not well described (e.g. Godeferd & Cambon 1994; Cambon 2002).

However, the nonlinear vortex-mode equation derived under the assumption of hydrostatic balance between the perturbation density and pressure is quantitatively applicable only when the ratio of vertical to horizontal velocity is extremely small ($u_3/u_1 = \alpha Fr^2$, where $\alpha = l_3/l_1$ is the ratio of vertical length scale to horizontal length scale). This is not consistent with most experiments and DNS, which usually show that $u_3/u_1 \geqslant 0.5$ (e.g. Itsweire, Helland & Van Atta 1986; Métais & Herring 1989). By contrast the ratio is $u_3/u_1 \sim \alpha$ in the linear wave-mode equation, which is consistent with RDT.

Note that the wave mode and vortex mode can be described directly by using the Craya–Herring frame (Métais & Herring 1989; Herring & Métais 1989) and the behaviours of these two modes become clearer in that frame. But we use in this study the usual Cartesian frame so that the comparison with the previous experiments and most of the DNS can be made directly. The results in the Craya–Herring frame can be reproduced by rotating the coordinates in the spectral space. Indeed, from our results in the Cartesian coordinates (Hanazaki & Hunt 1999, 2001), Salhi (2002) derived corresponding RDT solutions in the Craya–Herring frame.

In many experiments and observations in the ocean, horizontal motion leads to slow changes of the mean flow so that $N(x_3)$ or $\mathrm{d}U_1/\mathrm{d}x_3$ may no longer be constant. In that case, the assumptions of constant N and α in our RDT equations will not

be satisfied. But RDT can be applied as a 'local' model to the various mean flow conditions, as demonstrated by Galmiche & Hunt (2002).

3. Inviscid fluid

3.1. *Calculation for spectra*

The RDT equations have time-dependent coefficients when the flow has mean shear and it becomes difficult to obtain the general solution. However, the equations for $\hat{u}_3$ and $\hat{\rho}$ do not contain $\hat{u}_1$ and $\hat{u}_2$ so that those two equations can be solved separately. Eliminating $\hat{u}_3$, we obtain a single equation for $\hat{\rho}$ as

$$\left(k_{10}^2 + k_{20}^2 + (k_{30} - \alpha t k_{10})^2\right)\frac{\mathrm{d}^2\hat{\rho}}{\mathrm{d}t^2} - 2\alpha k_{10}(k_{30} - \alpha t k_{10})\frac{\mathrm{d}\hat{\rho}}{\mathrm{d}t} + \left(k_{10}^2 + k_{20}^2\right)N^2\hat{\rho} = 0. \quad (3.1)$$

This equation belongs to the type which can generally be solved by the Euler transform in the complex plane (e.g. Ince 1956). But here we derive a solution by a simpler variable transform which has been verified *a posteriori*.

We notice that equation (3.1) becomes a Legendre equation

$$(1 - z^2)\frac{\mathrm{d}^2\hat{\rho}}{\mathrm{d}z^2} - 2z\frac{\mathrm{d}\hat{\rho}}{\mathrm{d}z} + \nu(\nu + 1)\hat{\rho} = 0, \quad (3.2)$$

if we put

$$\begin{aligned} z(t) &= \mathrm{i}\frac{k_{30} - \alpha t k_{10}}{\left(k_{10}^2 + k_{20}^2\right)^{1/2}} = \mathrm{i}(\cot\theta_0 - \alpha t\cos\phi_0) \\ &= \mathrm{i}\frac{k_3(t)}{k_H} = \mathrm{i}\cot\theta(t), \end{aligned} \quad (3.3)$$

and select ν as

$$\nu(\nu + 1) = -\frac{\left(k_{10}^2 + k_{20}^2\right)N^2}{\alpha^2 k_{10}^2}, \quad (3.4)$$

i.e.

$$\nu = \frac{1}{2}\left[-1 \pm \left(1 - 4\frac{\left(k_{10}^2 + k_{20}^2\right)N^2}{\alpha^2 k_{10}^2}\right)^{1/2}\right] = \frac{1}{2}\left[-1 \pm \left(1 - 4\frac{Ri}{\cos^2\phi_0}\right)^{1/2}\right]. \quad (3.5)$$

The solution consists of two Legendre functions of the first and second kind, i.e. P_{ν_1} and Q_{ν_1}. Since the two possible values of ν, i.e. ν_1 and ν_2 which take the sign of $+$ and $-$ respectively in (3.5), satisfy the relation $\nu_2 = -\nu_1 - 1$, the general relations between the Legendre functions $Q_{\nu_1} = P_{-\nu_1-1} = P_{\nu_2}$ and $Q_{\nu_2} = P_{-\nu_2-1} = P_{\nu_1}$ show that the solution is independent of the choice of ν. That is, we can for example alternatively choose P_{ν_2} and Q_{ν_2} as a solution. The Legendre function with order ν of the form $\nu = -(1/2) \pm \mathrm{i}\mu$, where μ is a real number, is called a conical function or a Mehler function. Our solutions become conical functions when $Ri > 1/4$ for all ϕ_0, and when $Ri < 1/4$ for restricted angles which satisfy $(1/4)\cos^2\phi_0 < Ri$. Therefore, the analytical solutions of the RDT equation are in general described by the Legendre functions of complex degree with pure imaginary argument, and the linearly stable aspects of the flow are in particular described by the conical function. We hereafter use ν to represent ν_1, and then write the solution as

$$\hat{\rho}(t) = A P_\nu(z) + B\, Q_\nu(z), \quad (3.6)$$

and substitute (3.6) into (2.2) to obtain $\hat{u}_3$ as

$$\hat{u}_3(t) = -\frac{\mathrm{i}\alpha\cos\phi_0}{N^2}(AP'_\nu(z) + BQ'_\nu(z)). \tag{3.7}$$

Here, A and B are constants determined from the initial conditions $\hat{\rho}_0$ and $\hat{u}_{30}$, i.e.

$$A = \frac{1}{\sin^2\theta_0}Q'_\nu(z_0)\hat{\rho}_0 + \frac{N^2}{\mathrm{i}\alpha\cos\phi_0\sin^2\theta_0}Q_\nu(z_0)\hat{u}_{30}, \tag{3.8}$$

$$B = -\frac{1}{\sin^2\theta_0}P'_\nu(z_0)\hat{\rho}_0 - \frac{N^2}{\mathrm{i}\alpha\cos\phi_0\sin^2\theta_0}P_\nu(z_0)\hat{u}_{30}, \tag{3.9}$$

where $z_0 = z(0) = \mathrm{i}\cot\theta_0$ denotes the initial value of z and the primes denote differentiation by z, i.e.

$$P'_\nu(z_0) = \left.\frac{\mathrm{d}P_\nu}{\mathrm{d}z}\right|_{z=z_0}. \tag{3.10}$$

Next we calculate the three-dimensional spectra. In this study we assume that the initial density fluxes are zero, i.e.

$$\Phi_{\rho i}(\boldsymbol{k}_0, 0) = \frac{1}{2}\overline{\hat{\rho}_0^*\hat{u}_{i0} + \hat{\rho}_0\hat{u}_{i0}^*} = 0 \qquad (i = 1, 2, 3). \tag{3.11}$$

Then, we obtain

$$\begin{aligned}\Phi_{\rho 3}(\boldsymbol{k}(t), t) &= \frac{1}{2}\overline{\hat{\rho}^*\hat{u}_3 + \hat{\rho}\hat{u}_3^*} \\ &= \mathrm{Re}\Bigg[\frac{\mathrm{i}\alpha\cos\phi_0}{N^2\sin^4\theta_0}(P_\nu(z)Q'_\nu(z_0) - P'_\nu(z_0)Q_\nu(z)) \\ &\quad\times(P'_\nu(z)Q'_\nu(z_0) - P'_\nu(z_0)Q'_\nu(z))^*\Phi_{\rho\rho}(\boldsymbol{k}_0, 0) \\ &\quad+\frac{\mathrm{i}N^2}{\alpha\sin^4\theta_0\cos\phi_0}(P_\nu(z)Q_\nu(z_0) - P_\nu(z_0)Q_\nu(z)) \\ &\quad\times(P'_\nu(z)Q_\nu(z_0) - P_\nu(z_0)Q'_\nu(z))^*\Phi_{33}(\boldsymbol{k}_0, 0)\Bigg],\end{aligned} \tag{3.12}$$

$$\begin{aligned}\Phi_{33}(\boldsymbol{k}(t), t) = \frac{1}{\sin^4\theta_0}&|P'_\nu(z)Q_\nu(z_0) - P_\nu(z_0)Q'_\nu(z)|^2\,\Phi_{33}(\boldsymbol{k}_0, 0) \\ &+\frac{\alpha^2\cos^2\phi_0}{N^4\sin^4\theta_0}|P'_\nu(z)Q'_\nu(z_0) - P'_\nu(z_0)Q'_\nu(z)|^2\,\Phi_{\rho\rho}(\boldsymbol{k}_0, 0),\end{aligned} \tag{3.13}$$

$$\begin{aligned}\Phi_{\rho\rho}(\boldsymbol{k}(t), t) = \frac{1}{\sin^4\theta_0}&|P_\nu(z)Q'_\nu(z_0) - P'_\nu(z_0)Q_\nu(z)|^2\,\Phi_{\rho\rho}(\boldsymbol{k}_0, 0) \\ &+\frac{N^4}{\alpha^2\sin^4\theta_0\cos^2\phi_0}|P_\nu(z)Q_\nu(z_0) - P_\nu(z_0)Q_\nu(z)|^2\,\Phi_{33}(\boldsymbol{k}_0, 0),\end{aligned} \tag{3.14}$$

where the asterisks denote the complex conjugates. These expressions show that the three-dimensional spectra are determined by Ri and αt, which are contained in ν and z respectively.

Since the turbulence is initially nearly isotropic in usual laboratory experiments on grid turbulence and in DNS, we consider initially isotropic turbulence in this study. Then, the initial three-dimensional spectra are given by (Batchelor 1953)

$$\Phi_{ij}(\boldsymbol{k}_0, 0) = \frac{E(k_0)}{4\pi k_0^2}\left(\delta_{ij} - \frac{k_{i0}k_{j0}}{k_0^2}\right), \tag{3.15}$$

and

$$\Phi_{\rho\rho}(\boldsymbol{k}_0, 0) = \frac{S(k_0)}{4\pi k_0^2} 2N^2, \tag{3.16}$$

where

$$KE_0 = \int_0^\infty E(k_0)\,\mathrm{d}k_0 \tag{3.17}$$

and

$$PE_0 = \frac{1}{2N^2}\int \Phi_{\rho\rho}(\boldsymbol{k}_0, 0)\,\mathrm{d}\boldsymbol{k}_0 = \int_0^\infty S(k_0)\,\mathrm{d}k_0 \tag{3.18}$$

are the initial turbulent kinetic and potential energy.

3.2. *Variances and covariances*

Using (3.15)–(3.18) and noting that the integration by k_0 can be done separately, we obtain the vertical flux of density as

$$\begin{aligned}
\overline{\rho u_3}(t) &= \int \Phi_{\rho 3}(\boldsymbol{k}(t), t)\,\mathrm{d}\boldsymbol{k}_0 \\
&= \int_0^\infty k_0^2\,\mathrm{d}k_0 \int_0^\pi \sin\theta_0\,\mathrm{d}\theta_0 \int_0^{2\pi} \mathrm{d}\phi_0 \Phi_{\rho 3}(\boldsymbol{k}(t), t) \\
&= \frac{\alpha}{2\pi} PE_0 \int \mathrm{d}\theta_0\,\mathrm{d}\phi_0 \frac{\cos\phi_0}{\sin^3\theta_0} \\
&\quad \times \mathrm{Re}[\mathrm{i}(P_\nu(z)Q'_\nu(z_0) - P'_\nu(z_0)Q_\nu(z))(P'_\nu(z)Q'_\nu(z_0) - P'_\nu(z_0)Q'_\nu(z))^*] \\
&\quad + \frac{\alpha}{4\pi} RiKE_0 \int \mathrm{d}\theta_0\,\mathrm{d}\phi_0 \frac{1}{\sin\theta_0\cos\phi_0} \\
&\quad \times \mathrm{Re}[\mathrm{i}(P_\nu(z)Q_\nu(z_0) - P_\nu(z_0)Q_\nu(z))(P'_\nu(z)Q_\nu(z_0) - P_\nu(z_0)Q'_\nu(z))^*].
\end{aligned} \tag{3.19}$$

Other variances and covariances can be calculated similarly and the results are

$$\begin{aligned}
\overline{\rho^2}(t) &= \frac{N^2}{2\pi} PE_0 \int \mathrm{d}\theta_0\,\mathrm{d}\phi_0 \frac{1}{\sin^3\theta_0} \left|P_\nu(z)Q'_\nu(z_0) - P'_\nu(z_0)Q_\nu(z)\right|^2 \\
&\quad + \frac{N^2}{4\pi} RiKE_0 \int \mathrm{d}\theta_0\,\mathrm{d}\phi_0 \frac{1}{\sin\theta_0\cos^2\phi_0} \left|P_\nu(z)Q_\nu(z_0) - P_\nu(z_0)Q_\nu(z)\right|^2,
\end{aligned} \tag{3.20}$$

$$\begin{aligned}
\overline{u_3^2}(t) &= \frac{1}{2\pi Ri} PE_0 \int \mathrm{d}\theta_0\,\mathrm{d}\phi_0 \frac{\cos^2\phi_0}{\sin^3\theta_0} \left|P'_\nu(z)Q'_\nu(z_0) - P'_\nu(z_0)Q'_\nu(z)\right|^2 \\
&\quad + \frac{1}{4\pi} KE_0 \int \mathrm{d}\theta_0\,\mathrm{d}\phi_0 \frac{1}{\sin\theta_0} \left|P'_\nu(z)Q_\nu(z_0) - P_\nu(z_0)Q'_\nu(z)\right|^2.
\end{aligned} \tag{3.21}$$

We observe clearly that the time development of the variances and the covariances, such as the kinetic and potential energies and the vertical density flux, are determined by the initial total kinetic (KE_0) and potential (PE_0) energies and not by their specific spectral forms when the fluid is inviscid. This is the same as for stratified turbulence with no shear (Hanazaki & Hunt 1996). Since the expressions contain ν and z, the functional forms are determined by Ri and αt, similarly to the three-dimensional spectra.

The Reynolds stress $\overline{u_1 u_3}$ was calculated numerically in this study (cf. figure 3) by solving a set of equations for the three-dimensional spectra Φ_{ij} etc. and then integrating the obtained Φ_{13} in the spectral space.

We should note that for the spectral components of $\cos\phi = \cos\phi_0 = 0$ ($k_1 = k_{10} = 0$), three-dimensional spectra are identical to the no-shear results since α is always coupled with $k_1 (= k_{10})$ in (3.1). For example, the spectrum for the vertical density flux becomes

$$\Phi_{\rho 3}(\boldsymbol{k}(t), t) = -\frac{\sin\theta}{2N}\Phi_{\rho\rho}(\boldsymbol{k}_0, 0)\sin(2Nt\sin\theta) + \frac{N}{2\sin\theta}\Phi_{33}(\boldsymbol{k}_0, 0)\sin(2Nt\sin\theta), \quad (3.22)$$

in agreement with the no-shear solution (Hanazaki & Hunt 1996).

Therefore, if the energies and the fluxes have dominant contributions from the spectral components of $\cos\phi \sim 0$ ($\phi \sim \pi/2, 3\pi/2$), they will oscillate with period π/N just like no-shear flow, as will be illustrated later in figures 6 and 8. The dominance of components of $\phi = \pi/2, 3\pi/2$ in the energies and the Reynolds stresses at large times has been discussed by Moffatt (1967) for unstratified inviscid shear flow, noting that contribution from the distorted spectrum of the initial vertical kinetic energy $\Phi_{33}(\boldsymbol{k}_0, 0)$ dominates the integral for the Reynolds stress $-\overline{u_1 u_3}$, although more detailed analysis has been necessary in the evaluation of the integral, as noted later by Rogers (1991).

We should also note that this part of the spectrum is free from the additional viscous damping enhanced by the shear (cf. § 4), and will become increasingly dominant as time elapses.

The radial spectrum and the horizontal spectrum are also often dominated by the same components, although the vertical spectrum is dominated by different components ($\cos\phi < 0$, cf. § 5 and figure 20).

From (2.1) and (2.2) we can derive the following useful general relations among the three-dimensional spectra directly:

$$\left(\frac{\mathrm{d}}{\mathrm{d}t} + 2\nu k^2\right)\sum_i \Phi_{ii} = -2\alpha\Phi_{13} - 2\Phi_{\rho 3}, \quad (3.23)$$

$$\left(\frac{\mathrm{d}}{\mathrm{d}t} + 2\kappa k^2\right)\Phi_{\rho\rho} = 2N^2\Phi_{\rho 3}. \quad (3.24)$$

These equations show that $\overline{u_1 u_3}$ extracts kinetic energy from the mean shear, while the potential energy is supplied only by the exchange of $\overline{\rho u_3}$ with the kinetic energy. Adding these two equations and integrating, we obtain the total energy budget equation for the inviscid fluid as

$$KE(t) + PE(t) = -\alpha\int_0^t \overline{u_1 u_3}\,\mathrm{d}t + KE_0 + PE_0. \quad (3.25)$$

3.3. *Short-time approximations*

When $\alpha t \ll 1$ (and $Nt \ll 1$, with the assumption of $Ri = N^2/\alpha^2 \leqslant O(1)$), we expand $P_\nu(z)$, $P'_\nu(z)$, $Q_\nu(z)$ and $Q'_\nu(z)$ around z_0 in (3.21) and (3.22), use the fundamental relations between the Legendre functions such as $P_\nu(z)Q'_\nu(z) - P'_\nu(z)Q_\nu(z) = 1/(1-z^2)$ and its derivatives, then integrate analytically to obtain the short-time approximations. The results for $\overline{\rho^2}(t)$ and $\overline{u_3^2}(t)$ ($\alpha t \ll 1, Nt \ll 1$) after rather lengthy calculations are

$$\overline{\rho^2}(t) = 2N^2\left[PE_0 + \frac{1}{3}(Nt)^2(KE_0 - 2PE_0) - \frac{4}{45}(Nt)^4(KE_0 - 2PE_0) - \frac{2}{105}(Nt)^2(\alpha t)^2(KE_0 - 3PE_0)\right], \quad (3.26)$$

and

$$\overline{u_3^2}(t) = \frac{2}{3}KE_0 - \frac{8}{15}(Nt)^2(KE_0 - 2PE_0) - \frac{8}{105}(\alpha t)^2 KE_0. \quad (3.27)$$

Note that for $Nt \sim 1$ or $t \sim 1/N$, when $\alpha/N = Ri^{1/2} \geqslant 0.25$, $\overline{u_3^2}$ decreases more rapidly with shear. These results suggest that the energy ratio ER of potential energy to vertical kinetic energy (VKE), i.e. $ER \equiv PE/VKE = (\overline{\rho^2}/2N^2)/(\overline{u_3^2}/2)$ in the long-time limit is different from the value for stratified flow without mean shear ($=3/2$) since the terms containing α have coefficients different from $KE_0 - 2PE_0$. In stratified or stratified–rotating flow without mean shear, initially isotropic turbulence which satisfies $KE_0 - 2PE_0 = 3VKE_0 - 2PE_0 = 0$ does not lead to any energy exchange at any later time, showing that the initial condition $ER_0 \equiv PE_0/VKE_0 = 3/2$ corresponds to the final equilibrium state of turbulence (Hanazaki & Hunt 1996; Hanazaki 2002). Indeed, numerical simulations for stratified turbulence with such initial conditions showed very small vertical density flux, independent of whether there is a system rotation or not (Ramsden & Holloway 1992). In the stratified shear flow, the terms coupled with αt have different coefficients, showing that the mean shear modifies the partition among the energies. We finally note that equation (3.27) reduces to the results by Stretch (1986) and Derbyshire & Hunt (1992) if we substitute $PE_0 = 0$.

Differentiating (3.26) by time t, the vertical density flux can be obtained as

$$\begin{aligned}\overline{\rho u_3}(t) &= \frac{1}{2N^2}\frac{\mathrm{d}\overline{\rho^2}}{\mathrm{d}t} \\ &= \frac{2}{3}N^2 t(KE_0 - 2PE_0) - \frac{16}{45}N^4 t^3(KE_0 - 2PE_0) - \frac{8}{105}N^2\alpha^2 t^3(KE_0 - 3PE_0).\end{aligned} \tag{3.28}$$

From (3.26)–(3.28), the short-time approximation for the normalized vertical density flux when $c \equiv PE_0/KE_0 = (1/3)ER_0$ ($ER_0 \neq 0, \infty$) becomes

$$\begin{aligned}\frac{\overline{\rho u_3}}{\overline{\rho^2}^{1/2}\overline{u_3^2}^{1/2}} = \left(\frac{1}{3c}\right)^{1/2}(Nt)\Bigg[1 - 2c + \frac{2}{35}(\alpha t)^2(4c-1) \\ - (1-2c)(Nt)^2\left(\frac{8}{15} + \left(\frac{1}{6c} - \frac{2}{5}\right)(1-2c)\right)\Bigg].\end{aligned} \tag{3.29}$$

This or (3.28) shows that whether $c < 1/2$ or $c > 1/2$, or equivalently $ER_0 < 3/2$ or $ER_0 > 3/2$, determines the initial sign of the vertical density flux. This is the same as for the stratified flow without mean shear (Hanazaki & Hunt 1996). Gerz *et al.* (1989) considered the effect of ER_0 and computed the case of $ER_0 = Ri$, for which (3.29) at the leading order gives $(1 - 2Ri/3)\alpha t$. Their results also show that the initial vertical density flux is smaller for larger $Ri(\leqslant 1)$, in agreement with this prediction.

We note, however, that even when $c = 1/2$ ($ER_0 = 3/2$), the flux increases slowly with time due to the mean shear, since for this initial condition

$$\frac{\overline{\rho u_3}}{\overline{\rho^2}^{1/2}\overline{u_3^2}^{1/2}} = \left(\frac{2}{3}\right)^{1/2}\frac{2}{35}(\alpha t)^2(Nt), \tag{3.30}$$

and the flux changes at $O(t^3)$. This is different from the no-shear flow due to the last term on the right-hand side of equation (3.26). It is of $O(t^3)$ and the growth would be slow. We also note in (3.29) that the initial time development is determined predominantly by Nt except when $c = 1/2$ and the effect of shear appears only at a higher order.

When there is no initial potential energy ($c=0$, i.e. $PE_0=0$), the initial time development of the normalized flux becomes

$$\frac{\overline{\rho u_3}}{\overline{\rho^2}^{1/2}\overline{u_3^2}^{1/2}} = 1 - \frac{1}{35}(\alpha t)^2 + O(t^4) = 1 - \frac{1}{35Ri}(Nt)^2 + O(t^4), \tag{3.31}$$

which reduces to $\overline{\rho u_3}/(\overline{\rho^2}^{1/2}\overline{u_3^2}^{1/2})(t\to 0)=1$ when $\alpha=0$, in agreement with stratified turbulence without mean shear (Hanazaki & Hunt 1996). This shows that, if $PE_0=0$, the initial time development of the vertical density flux is controlled by αt, not by Nt, in contrast to the general case of $PE_0\neq 0$. This will be illustrated in figure 1, where the time development of $\overline{\rho u_3}/\left(\overline{\rho^2}\,\overline{u_3^2}\right)^{1/2}$ is plotted against αt, which gives the same value for $\alpha t<1$, independent of Ri. On the other hand, the plot against Nt (figure 8) shows that at smaller Ri there is significant decrease in the normalized flux when $Nt<1$.

However, when there is no initial kinetic energy ($KE_0=0$, i.e. $c=\infty$), the initial value of the normalized flux becomes

$$\frac{\overline{\rho u_3}}{\overline{\rho^2}^{1/2}\overline{u_3^2}^{1/2}}(t\to 0) = -\left(\frac{5}{6}\right)^{1/2}, \tag{3.32}$$

again in agreement with stratified flow without mean shear (Gerz & Yamazaki 1993; Hanazaki & Hunt 1996).

The energy ratio ER of the potential energy PE to the vertical kinetic energy VKE has a short-time approximation

$$ER = 3c + (Nt)^2(1-2c)\left(1+\frac{12}{5}c\right) + \frac{12}{35}c(\alpha t)^2 + O(t^4), \tag{3.33}$$

for $c\neq 0,\infty$. The initial increase or decrease is determined by whether $c<1/2$ or $c>1/2$, in accordance with the sign of the vertical density flux (cf. (3.29)).

When $c=0$ ($PE_0=0$),

$$\begin{aligned} ER &= (Nt)^2\left(1+\frac{8}{5}(Nt)^2+\frac{2}{35}(\alpha t)^2+\cdots\right) \\ &= Ri(\alpha t)^2\left(1+\frac{8}{5}Ri(\alpha t)^2+\frac{2}{35}(\alpha t)^2+\cdots\right), \end{aligned} \tag{3.34}$$

When $c=\infty$ ($KE_0=0$),

$$ER = \frac{15}{8}(Nt)^{-2}\left(1-\frac{2}{3}(Nt)^2+\frac{8}{45}(Nt)^2+\frac{2}{35}(\alpha t)^2+\cdots\right). \tag{3.35}$$

These results show that the leading-order term is always determined by Nt and if we plot the time development of ER against Nt, ER is independent of Ri, while if we plot against αt, ER is proportional to Ri. Examples for $PE_0=0$ are given in figures 4 and 6 of this paper and figure 18 of Holt *et al.* (1992), and examples for $KE_0=0$ are given by the dashed lines in figure 11 ($Nt<1$) of this paper.

The above results for $Ri\leqslant O(1)$ show that the effect of shear is generally weak compared to the stratification effects during the initial time development because in most cases shear appears at higher order of t in the expansion. However, with very strong shear ($Ri\ll 1$), the effect of shear may become comparable to the stratification effects even in the initial time development.

4. Effects of viscosity and diffusion

With non-zero viscosity and diffusion, the solutions of (2.1) and (2.2) generally become much more complicated, but if the Prandtl number $Pr(=\nu/\kappa)$ is equal to 1, the solutions take a much simpler form given by

$$\hat{u_i} = D(t)\hat{u}_{i\,\mathrm{inv}} \quad (i = 1, 2, 3), \tag{4.1}$$

and

$$\hat{\rho} = D(t)\hat{\rho}_{\mathrm{inv}}, \tag{4.2}$$

where subscript inv denotes the inviscid solutions. Here, $D(t)$ is a function which satisfies

$$\left(\frac{\mathrm{d}}{\mathrm{d}t} + \nu k^2\right) D = 0, \tag{4.3}$$

with initial condition $D(0) = 1$, and is given by

$$D(t) = \exp\left(-\nu \int_0^t k^2 \,\mathrm{d}t\right) = \exp\left(-\nu t\left(k_0^2 - \alpha t k_1 k_{30} + \frac{1}{3}(\alpha t)^2 k_1^2\right)\right), \tag{4.4}$$

in agreement with the effects of viscosity on the shear flow without stratification (Townsend 1976). Note that D is a function of both t and $\boldsymbol{k}_0$, but to clarify that it is a solution of an ordinary differential equation (4.3), it is represented by $D(t)$.

Then, for example, the inviscid three-dimensional spectra $\Phi_{\rho 3}(\boldsymbol{k}, t)_{\mathrm{inv}}$ should be multiplied by

$$\begin{aligned} D^2(t) &= \exp\left(-2\nu t\left(k_0^2 - \alpha t k_1 k_{30} + \frac{1}{3}(\alpha t)^2 k_1^2\right)\right) \\ &= \exp\left(-2\nu t k_0^2\left(1 - \alpha t \sin\theta_0 \cos\theta_0 \cos\phi_0 + \frac{1}{3}(\alpha t)^2 \sin^2\theta_0 \cos^2\phi_0\right)\right), \end{aligned} \tag{4.5}$$

to give the viscous and diffusive ($Pr = 1$) spectrum as

$$\Phi_{\rho 3}(\boldsymbol{k}, t) = \Phi_{\rho 3}(\boldsymbol{k}, t)_{\mathrm{inv}} D^2(t). \tag{4.6}$$

Although the results in this study are limited to $Pr = 1$, all the previous DNS for stratified shear flow have also been done for $Pr = 1$ and direct comparison with them is possible; and most of the results for $Pr = 1$ would be applicable also to the case of $Pr \neq 1$, except for the details of the unsteady aspects of the spectra and the final decaying and layering processes which have been investigated by Pearson & Linden (1983) and Hanazaki & Hunt (1996) for stratified unsheared turbulence.

In this study a viscosity term with real molecular viscosity coefficient is used to describe the viscous damping. In previous studies large artificial turbulent viscosity coefficients (Townsend 1976; Salhi & Cambon 1997) or the Rayleigh friction proportional to the velocity (Hunt *et al.* 1988), has been used to model the rapid initial decay $\propto t^{-1}$ ($Nt < 1$) as observed in the grid turbulence. For these methods the comparison with experiments is better under an implicit assumption that significant energy decay at large scales is due to the nonlinear energy transfer to small scales. However, DNS (e.g. Gerz & Yamazaki 1993) usually does not show such a rapid decay and since inclusion of such 'modelling' will further complicate the interpretation of results, we do not use those methods in this study.

The calculation of the energy and the fluxes (3.20)–(3.22) requires integrations such as

$$\overline{\rho u_3}(t) = \int_0^\infty k_0^2\,\mathrm{d}k_0 \int_0^\pi \sin\theta_0\,\mathrm{d}\theta_0 \int_0^{2\pi} \mathrm{d}\phi_0 \Phi_{\rho 3}(\boldsymbol{k}, t)_{\mathrm{inv}} D^2(t), \tag{4.7}$$

where integration by k_0 involves the separate integrals

$$\int_0^\infty \mathrm{d}k_0 E(k_0) D^2(t), \quad \int_0^\infty \mathrm{d}k_0 S(k_0) D^2(t). \tag{4.8}$$

Then, if the initial energy spectrum is given by

$$E(k_0) = KE_0 \frac{4}{\sqrt{\pi}} \frac{k_0^2}{k_p^3} \exp\left(-k_0^2/k_p^2\right), \tag{4.9}$$

which gives $E(k_0) \propto k_0^2$ for $k_0/k_p \ll 1$ as in the experiments, the first integral of (4.8) becomes

$$KE_0 \frac{1}{\left[1 + 2\nu t k_p^2 \left(1 - \alpha t \sin\theta_0 \cos\theta_0 \cos\phi_0 + \frac{1}{3}(\alpha t)^2 \sin^2\theta_0 \cos^2\phi_0\right)\right]^{3/2}}, \tag{4.10}$$

where the term containing $\nu t k_p^2$ in the denominator denotes the viscosity effect.

On the other hand, if the initial energy spectrum is given by

$$E(k_0) = KE_0 \left(\frac{2}{9\pi}\right)^{1/2} \left(\frac{2}{k_p}\right)^5 k_0^4 \exp\left(-2k_0^2/k_p^2\right), \tag{4.11}$$

which gives $E(k_0) \propto k_0^4$ for $k_0/k_p \ll 1$ (Saffman 1967) as has been often used in DNS to model the final decay of turbulence, integration of $E(k_0)D^2(t)$ by k_0 gives

$$KE_0 \frac{1}{\left[1 + \nu t k_p^2 \left(1 - \alpha t \sin\theta_0 \cos\theta_0 \cos\phi_0 + \frac{1}{3}(\alpha t)^2 \sin^2\theta_0 \cos^2\phi_0\right)\right]^{5/2}}. \tag{4.12}$$

Then, with viscosity and diffusion but for $Pr = 1$, KE_0 and PE_0 in (3.20)–(3.22) are replaced by functions of the form (4.10) or (4.12), which should be integrated by θ_0 and ϕ_0. For example, if the initial energy spectrum $E(k_0)$ is given by (4.11), the energies and the flux for a viscous and diffusive fluid ($Pr = 1$) become

$$\begin{aligned}
\overline{\rho^2}(t) = {} & \frac{N^2}{2\pi} PE_0 \int_A \mathrm{d}\theta_0\,\mathrm{d}\phi_0 f_{\mathrm{vis}}(\theta_0, \phi_0) \frac{1}{\sin^3\theta_0} \left|P_\nu(z)Q'_\nu(z_0) - P'_\nu(z_0)Q_\nu(z)\right|^2 \\
& + \frac{N^2}{4\pi} RiKE_0 \int_B \mathrm{d}\theta_0\,\mathrm{d}\phi_0 f_{\mathrm{vis}}(\theta_0, \phi_0) \frac{1}{\sin\theta_0 \cos^2\phi_0} \left|P_\nu(z)Q_\nu(z_0) - P_\nu(z_0)Q_\nu(z)\right|^2, \qquad (4.13) \\
\overline{u_3^2}(t) = {} & \frac{1}{2\pi Ri} PE_0 \int_C \mathrm{d}\theta_0\,\mathrm{d}\phi_0 f_{\mathrm{vis}}(\theta_0, \phi_0) \frac{\cos^2\phi_0}{\sin^3\theta_0} \left|P'_\nu(z)Q'_\nu(z_0) - P'_\nu(z_0)Q'_\nu(z)\right|^2 \\
& + \frac{1}{4\pi} KE_0 \int_D \mathrm{d}\theta_0\,\mathrm{d}\phi_0 f_{\mathrm{vis}}(\theta_0, \phi_0) \frac{1}{\sin\theta_0} \left|P'_\nu(z)Q_\nu(z_0) - P_\nu(z_0)Q'_\nu(z)\right|^2, \qquad (4.14)
\end{aligned}$$

and

$$\begin{aligned}
\overline{\rho u_3}(t) = {} & \frac{\alpha}{2\pi} PE_0 \int_E \mathrm{d}\theta_0\,\mathrm{d}\phi_0 f_{\mathrm{vis}}(\theta_0, \phi_0) \frac{\cos\phi_0}{\sin^3\theta_0} \\
& \times \mathrm{Re}[\mathrm{i}(P_\nu(z)Q'_\nu(z_0) - P'_\nu(z_0)Q_\nu(z))(P'_\nu(z)Q'_\nu(z_0) - P'_\nu(z_0)Q'_\nu(z))^*] \\
& + \frac{\alpha}{4\pi} RiKE_0 \int_F \mathrm{d}\theta_0\,\mathrm{d}\phi_0 f_{\mathrm{vis}}(\theta_0, \phi_0) \frac{1}{\sin\theta_0 \cos\phi_0} \\
& \times \mathrm{Re}[\mathrm{i}(P_\nu(z)Q_\nu(z_0) - P_\nu(z_0)Q_\nu(z))(P'_\nu(z)Q_\nu(z_0) - P_\nu(z_0)Q'_\nu(z))^*], \qquad (4.15)
\end{aligned}$$

where

$$f_{\rm vis}(\theta_0,\phi_0)=\frac{1}{\left[1+\nu t k_p^2\left(1-\alpha t\sin\theta_0\cos\theta_0\cos\phi_0+\frac{1}{3}(\alpha t)^2\sin^2\theta_0\cos^2\phi_0\right)\right]^{5/2}},\quad(4.16)$$

and A to F label the integrals for later discussions (§ 6) on the insensitivity of the energy ratio and normalized flux to initial energy partitions.

These results show that the decay rate of the energies and the fluxes indicated by the powers of $-3/2$ or $-5/2$ depends on the initial spectral forms of $E(k_0)$ and $S(k_0)$ for $k_0/k_p\ll 1$ as in the no-shear flow (Hanazaki & Hunt 1996). However, the decay also depends on the peak wavenumber k_p and the shear α, where the effect of the latter has a directional $(\theta_0-\phi_0)$ preference. In particular, when $k_1=k_{10}=0$ or equivalently $\cos\phi_0=0$, there is no additional viscous decay due to the shear, as already noted. Since ν is coupled only with α and not with N, the viscous decay is controlled only by the shear even in stratified fluid. This shows that energy decay is controlled by the initial spectra and shear even with stratification, and verifies the conjecture by Hunt *et al.* (1988) that decay would be mainly controlled by the shear.

We also note in (4.13)–(4.15) that the energies and the fluxes are proportional to KE_0 and PE_0 even in viscous fluids with $Pr=1$, showing that the energy spectral form is of secondary importance in determining the energy and the flux.

5. Spectra

One-dimensional spectra in the x_1-direction can be calculated as follows. First, we rewrite the inviscid three-dimensional spectrum such as $\Phi_{\rho 3}$ in the cylindrical coordinates (r,φ) which satisfy $k_2=r\cos\varphi$ and $k_3(t)=r\sin\varphi$, so that the one-dimensional spectrum becomes

$$\begin{aligned}\Theta_{\rho 3}(k_1,t)&=\int\Phi_{\rho 3}(\boldsymbol{k},t)\,{\rm d}k_2\,{\rm d}k_3(t)\\&=\int_0^\infty r\,{\rm d}r\int_0^{2\pi}{\rm d}\varphi\,\Phi_{\rho 3}(\boldsymbol{k},t).\end{aligned}\quad(5.1)$$

Here, the viscous three-dimensional spectrum which should be substituted into (5.1) is

$$\begin{aligned}\Phi_{\rho 3}(\boldsymbol{k},t)&=\Phi_{\rho 3}(\boldsymbol{k},t)_{\rm inv}D^2(t)\\&=\Phi_{\rho 3}(\boldsymbol{k},t)_{\rm inv}\exp\left(-2\nu t\left(k^2+\alpha t k_1k_3+\frac{1}{3}(\alpha t)^2k_1^2\right)\right)\\&=\Phi_{\rho 3}(\boldsymbol{k},t)_{\rm inv}\exp\left(-2\nu t\left(k_1^2+r^2+\alpha t k_1 r\sin\varphi+\frac{1}{3}(\alpha t)^2k_1^2\right)\right),\end{aligned}\quad(5.2)$$

with the inviscid three-dimensional spectrum given by

$$\begin{aligned}\Phi_{\rho 3}(\boldsymbol{k},t)_{\rm inv}=\mathrm{Re}\Bigg[&{\rm i}\frac{\alpha k_1}{4\pi\left(k_1^2+r^2\cos^2\varphi\right)^{1/2}}\Bigg(2\frac{k_1^2+r^2\cos^2\varphi+(r\sin\varphi+\alpha t k_1)^2}{\left(k_1^2+r^2\cos^2\varphi\right)^2}\\&\times(P_\nu(z)Q_\nu'(z_0)-P_\nu'(z_0)Q_\nu(z))(P_\nu'(z)Q_\nu'(z_0)-P_\nu'(z_0)Q_\nu'(z))^*\\&\times S\left(\left[k_1^2+r^2\cos^2\varphi+(r\sin\varphi+\alpha t k_1)^2\right]^{1/2}\right)\\&+\frac{Ri}{k_1^2}(P_\nu(z)Q_\nu(z_0)-P_\nu(z_0)Q_\nu(z))(P_\nu'(z)Q_\nu(z_0)-P_\nu(z_0)Q_\nu'(z))^*\\&\times E\left(\left[k_1^2+r^2\cos^2\varphi+(r\sin\varphi+\alpha t k_1)^2\right]^{1/2}\right)\Bigg)\Bigg],\end{aligned}\quad(5.3)$$

where

$$z(t) = \mathrm{i}\cot\theta = \mathrm{i}\frac{r\sin\varphi}{\left(k_1^2 + r^2\cos^2\varphi\right)^{1/2}}, \tag{5.4}$$

$$z_0 = \mathrm{i}\cot\theta_0 = \mathrm{i}(\cot\theta + \alpha t\cos\phi) = \mathrm{i}\frac{r\sin\varphi + \alpha t k_1}{\left(k_1^2 + r^2\cos^2\varphi\right)^{1/2}}, \tag{5.5}$$

and

$$\nu = \frac{1}{2}\left[-1 + \left(1 - \frac{4Ri\left(k_1^2 + r^2\cos^2\varphi\right)}{k_1^2}\right)^{1/2}\right]. \tag{5.6}$$

Three-dimensional radial spectra, such as $E_{33}(k)$ which gives vertical kinetic energy $(1/2)\overline{u_3^2} = \int_0^\infty E_{33}(k)\,\mathrm{d}k$, are calculated using

$$E_{33}(k) = E_{33}(|\boldsymbol{k}|) = \frac{1}{2}k^2\int \Phi_{33}(\boldsymbol{k}, t)\sin\theta\,\mathrm{d}\theta\,\mathrm{d}\phi, \tag{5.7}$$

where $\Phi_{33}(\boldsymbol{k}, t)$ is given in the distorted coordinates $(k(t), \theta(t), \phi)$ by

$$\begin{aligned}\Phi_{33}(\boldsymbol{k}, t) &= \Phi_{33}(\boldsymbol{k}, t)_{\mathrm{inv}} D^2(t)\\ &= \Phi_{33}(\boldsymbol{k}, t)_{\mathrm{inv}} e^{-2\nu t k^2\left(1+\alpha t\sin\theta\cos\theta\cos\phi + \frac{1}{3}(\alpha t)^2\sin^2\theta\cos^2\phi\right)}.\end{aligned} \tag{5.8}$$

Here, $\Phi_{33}(\boldsymbol{k}(t), t)_{\mathrm{inv}}$ must be rewritten in distorted coordinates as

$$\begin{aligned}\Phi_{33}(\boldsymbol{k}, t)_{\mathrm{inv}} = {} & \frac{\cos^2\phi}{2\pi Rik^2\sin^3\theta}\left(\sin^2\theta + (\cos\theta + \alpha t\sin\theta\cos\phi)^2\right)\\ & \times |P_\nu'(z)Q_\nu'(z_0) - P_\nu'(z_0)Q_\nu'(z)|^2 S(k[\sin^2\theta + (\cos\theta + \alpha t\sin\theta\cos\phi)^2]^{1/2})\\ & + \frac{1}{4\pi k^2\sin^2\theta}|P_\nu'(z)Q_\nu(z_0) - P_\nu(z_0)Q_\nu'(z)|^2\\ & \times E(k[\sin^2\theta + (\cos\theta + \alpha t\sin\theta\cos\phi)^2]^{1/2}),\end{aligned} \tag{5.9}$$

where

$$z(t) = \mathrm{i}\cot\theta, \quad z_0 = \mathrm{i}\cot\theta_0 = \mathrm{i}(\cot\theta + \alpha t\cos\phi), \tag{5.10}$$

and

$$\nu = \frac{1}{2}\left[-1 + \left(1 - \frac{4Ri}{\cos^2\phi}\right)^{1/2}\right]. \tag{5.11}$$

Other one-dimensional spectra and three-dimensional radial spectra can be calculated similarly using the inviscid three-dimensional spectra (3.12)–(3.14) and rewriting them using appropriate coordinates.

We should note here that, in the spectrum at large times, such as $E_{33}(k)$ for $\alpha t \gg 1$, the contribution of the initial spectrum given in the form of $E(k_0) = E(k[\sin^2\theta + (\cos\theta + \alpha t\sin\theta\cos\phi)^2]^{1/2})$ (cf. (5.9)) decreases rapidly except where $\sin\theta \ll 1$ or $|\cos\phi| \ll 1$. A similar discussion has been given in Hunt & Carruthers (1990). Finally, we mention that there is one exception to this, which occurs in the vertical spectrum where negative $\cos\phi$, or $\cos\phi = -1$ (i.e. $\phi = \pi$) becomes dominant (cf. figure 20, § 6).

6. Comparison with DNS and experiments

Figure 1 shows the time development of the normalized vertical density flux $\overline{\rho u_3}/(\overline{\rho^2}\,\overline{u_3^2})^{1/2}$ when $Pr = 1$, $PE_0 = 0$, $Re_0 = u_0 l_0/\nu = ((2/3)KE_0)^{1/2} l_0/\nu = 42.7$ and the

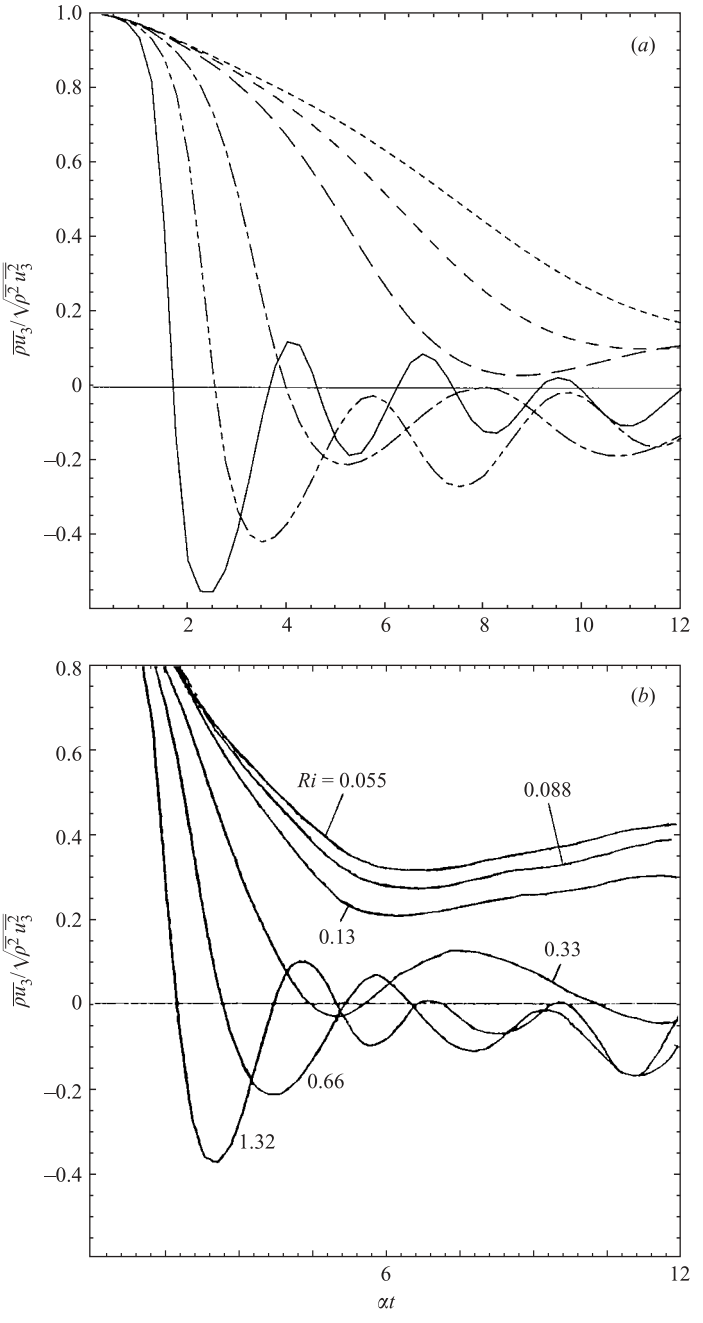

FIGURE 1. Time development of the normalized vertical density flux when $Pr = 1$, $KE_0 = 1.015$ and $PE_0 = 0$ with $E(k_0)$ given by (4.11). $\alpha = 2.729$, $k_p = 4$, $\nu = 0.01742$, $l_0 = 0.9044$, $Re_0 = u_0 l_0/\nu = ((2/3)KE_0)^{1/2} l_0/\nu = 42.7$. (*a*) RDT: ————, $Ri = 1.32$; — - - — - - —, $Ri = 0.66$; — - — - —, $Ri = 0.33$; — — —, $Ri = 0.13$; – – – –, $Ri = 0.0825$; ----------, $Ri = 0.055$. (*b*) DNS by Gerz & Schumann (1991).

initial kinetic energy spectrum $E(k_0)$ is given by (4.11) ($k_p = 4$). The conditions are the same as those used in DNS by Gerz & Shumann (1991). Comparison of the RDT results with DNS shows good agreement, including the oscillation period of

the flux and the appearance of the mainly persistent countergradient flux at large Richardson numbers ($Ri = 0.66, 1.32$). Although this effect has been identified by some other authors as a general characteristic of stratified 'shear' flow, we find that for larger Ri (> 1.0) the countergradient flux does not persist. As will be shown later in figure 8, the average flux will become nearly zero in the limit of $Ri \to \infty$ (no shear). The DNS results generally give a weaker countergradient flux than RDT, which could be attributable to nonlinear effects as discussed in previous studies on stratified turbulence without mean shear (Gerz & Yamazaki 1993; Hanazaki & Hunt 1996).

Figure 1(a) shows that the initial fluxes at the same αt (< 0.7) agree for different Ri (i.e. different N), showing that the initial time development is mainly determined by shear α under the condition of $PE_0 = 0$. These characteristics, which have also been observed in DNS (e.g. Holt *et al.* 1992, see their figure 15), can be explained by the short-time approximations of RDT for $PE_0 = 0$ described in (3.31).

We should note here that in DNS for different $Ri = N^2/\alpha^2$, N has usually been varied while α is kept constant. In Gerz & Shumann (1991), the initial shear number $Sh_0 = \alpha l_0/v_0$ defined by the initial integral scale l_0 and the initial r.m.s. velocity v_0 is kept constant, while the initial Froude number $Fr_0 = v_0/Nl_0$ is changed. Since these parameters have the relation $Ri = 1/(Fr_0 Sh_0)^2$, when Sh_0 is a constant, large Ri means small Fr_0, i.e. weaker nonlinearity. Therefore, larger Ri should give better agreement between RDT and DNS. In Gerz & Schumann (1991) where $Sh_0 = 3$, the formal applicability condition of RDT, i.e. $Fr_0 = 1/(Sh_0 Ri^{1/2}) < 1$ (Hanazaki & Hunt 1996) is satisfied for $Ri > 0.58$. This is consistent with the fact that good agreement between RDT and DNS is obtained for $Ri \geqslant 0.66$ in figure 1. In other words, even for the same Ri, simultaneous realization of stronger stratification (smaller Froude number Fr) and stronger shear (larger shear number Sh) leads to weaker nonlinearity. Therefore, it is important to know the values of Sh_0 (or α) and Fr_0 (or N) in addition to Ri to estimate the strength of the nonlinear effects in DNS. In DNS of Holt *et al.* (1992), the initial shear number is $Sh_0 = 0.6$, much lower than that used by Gerz & Schumann (1991), leading to stronger nonlinearity and a weaker countergradient density flux. In their study for $Pr = 1$, the minimum value of $\overline{\rho u_3}/(\overline{\rho^2}\,\overline{u_3^2})^{1/2}$ when $Ri = 1$ is -0.17, while in figure 1(b) (Gerz & Schumann 1991), stronger countergradient flux (~ -0.2) is achieved even at $Ri = 0.66$ although a special top-hat type initial energy spectrum $E(k_0)$ has been used by Holt *et al.* (1992).

Figure 2 shows the time development of the potential energy under the same conditions as figure 1. The agreement between RDT and DNS for large $Ri (\geqslant 0.33)$ is good. For small Richardson numbers ($Ri \leqslant 0.13$), the RDT predicts a monotonic decay, because RDT incorrectly predicts that the vertical velocity fluctuations are suppressed by shear (e.g. Hunt & Carruthers 1990; Lee, Kim & Moin 1990). The nonlinear transfer of energy between different flow directions is the reason why the DNS shows an increase in potential energy.

The momentum flux or Reynolds stress results in figure 3 show the same transition as the vertical density flux as Ri increases above ~ 0.1, when (for finite strain time αt) the structure of the fluctuations changes and the stress changes sign, and there is an oscillatory countergradient flux for a certain periods of time. As Ri increases further ($Ri > 0.33$) the Reynolds stress becomes permanently negative, but decreasing in magnitude. Thus the suppression of Reynolds stress by stable stratification for Ri greater than a critical value $Ri_{crit} \sim 0.3$ is in general not caused by suppression of linear instability. Rather, it is because the dynamics of the eddy structure changes as Ri increases above ~ 0.1 so as progressively to reduce the proportion of the time that

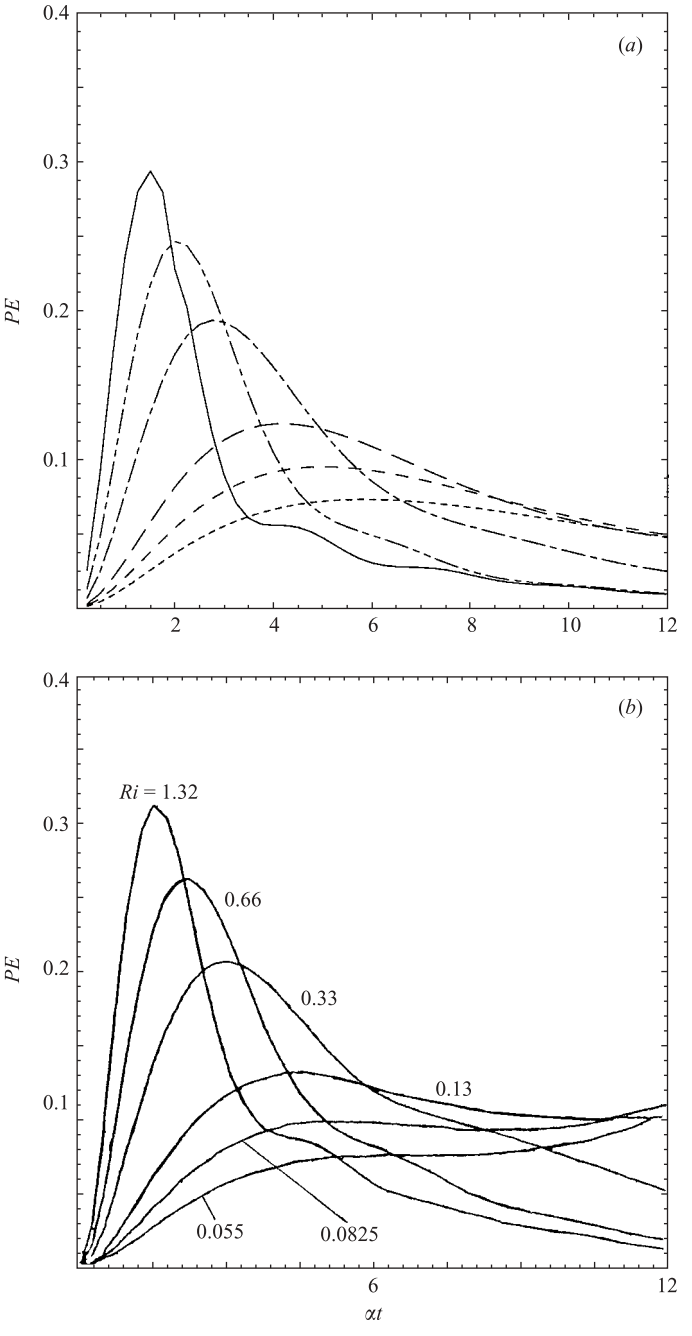

FIGURE 2. Time development of the potential energy PE under the same conditions as figure 1. (*a*) RDT; ————, $Ri = 1.32$; —·—·—·—, $Ri = 0.66$; —·—·—, $Ri = 0.33$; — — —, $Ri = 0.13$; – – – –, $Ri = 0.0825$; ----------, $Ri = 0.055$. (*b*) DNS by Gerz & Schumann (1991).

the Reynolds stress is positive. Therefore, the shear production of turbulent energy becomes negative, which rapidly reduces the vertical turbulence. As the analysis and DNS results of Galmiche & Hunt (2002) demonstrate, the effect of this on a typical mean velocity profile where $\mathrm{d}^2U/\mathrm{d}x_3^2 \neq 0$ is to change the mean flow profile

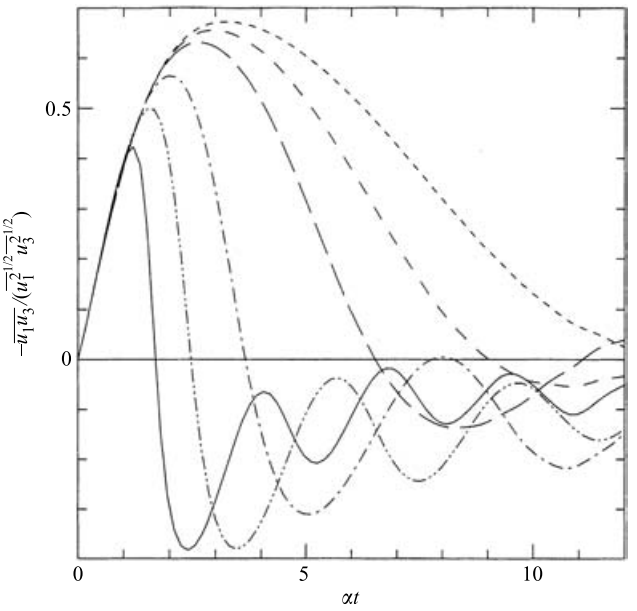

FIGURE 3. Time development of the Reynolds stress $-\overline{u_1u_3}/(\overline{u_1^2}^{1/2}\overline{u_3^2}^{1/2})$ obtained by RDT under the same conditions as figure 1. ————, $Ri=1.32$; — - - — - - —, $Ri=0.66$; — - — - —, $Ri=0.33$; — — —, $Ri=0.13$; – – – –, $Ri=0.0825$; ----------, $Ri=0.055$.

with a back reaction on the turbulence. It can lead to either a stable or unstable flow pattern depending on $\mathrm{d}\overline{\rho}/\mathrm{d}x_3$ and $\partial U_1/\partial x_3(x_3)$ (see also the conjectures of Derbyshire 1994)

Figure 4 shows the time development of the energy ratio $ER \equiv PE/VKE$ in stratified shear flow, where VKE is the vertical kinetic energy. The energy ratio ER at large times ($\alpha t \geqslant 10$) decreases for $Ri > 0.25$ with the increase of Ri. This tendency agrees with the DNS by Holt *et al.* (1992) for $Pr=1$ and $PE_0=0$, although they assumed a top-hat type initial kinetic energy spectrum as noted earlier. The specific values of $ER(Nt \gg 1$ or $\alpha t \gg 1)$ are also in good agreement between RDT and DNS for $Ri \geqslant 0.25$, as will be shown later in figure 11. Comparison of the RDT results for $Ri=0.25$ and $Ri=0.088$ suggests that at large αt ER is smaller for smaller Ri for low $Ri(<0.25)$. But longer time development (cf. figure 6) until $Nt=12$ ($\alpha t = Nt/Ri^{1/2} = 40.5$ when $Ri=0.088$) shows that for $Ri=0.088$ ER increases considerably with time and reaches its largest value, showing that the smallest value of Ri gives the largest ER over long times. This is different from the previous results of DNS and experiments (cf. figure 8 of Schumann & Gerz 1995). For example, DNS by Holt *et al.* (1992) shows that ER reaches its maximum at about $Ri=0.25$ and the value at $Ri=0.088$ is much smaller ($ER \sim 0.9$) at $\alpha t = 14$, although the DNS gives data only for $\alpha t \leqslant 14$ and longer time development might give somewhat different behaviour. When the Richardson number is small ($Ri < 0.25$), nonlinear effects lead to the potential energy PE becoming larger than for the linear prediction (cf. figure 2). But the vertical kinetic energy VKE is even greater as noted in the discussion of figure 2, implying that ER should be less than for the linear prediction. Previous studies do not give the associated time development of VKE.

Figure 5 shows that the inviscid results ($Re=\infty$) for ER give values about twice as high as for the case $Re \sim 43$ in figure 4, indicating that in shear flows, the ratios of

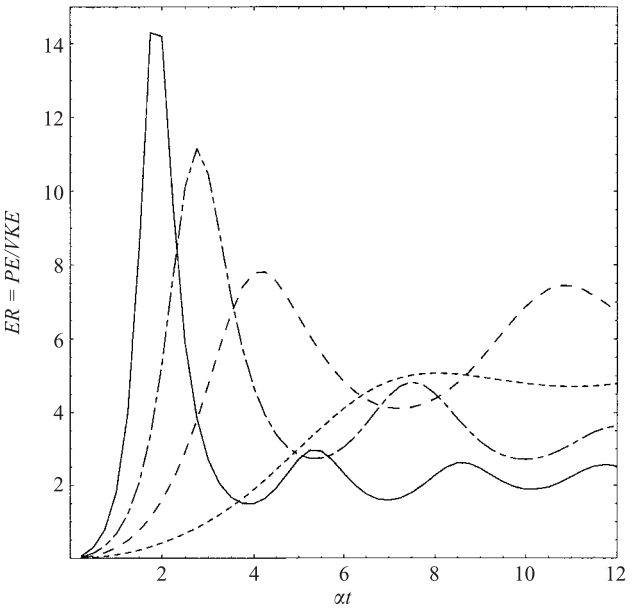

FIGURE 4. RDT results for the time development of energy ratio $ER = PE/VKE$ under the same conditions as figure 1. ————, $Ri = 1$; —·——·—, $Ri = 0.5$; – – – –, $Ri = 0.25$; ----------, $Ri = 0.088$.

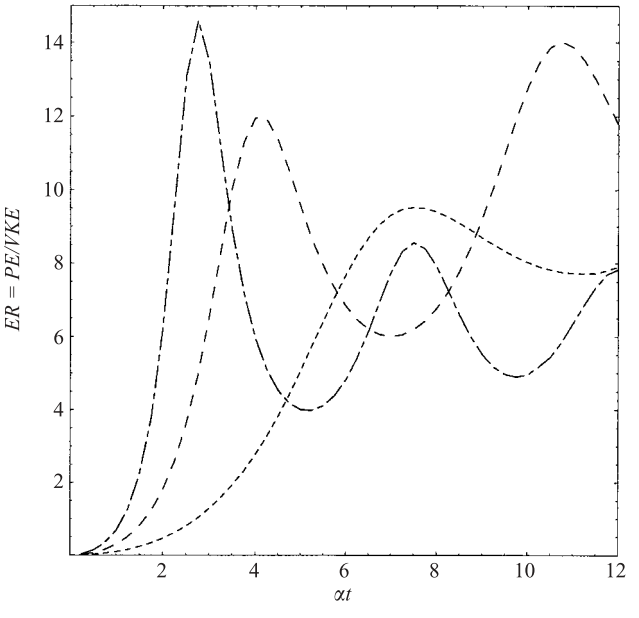

FIGURE 5. Inviscid RDT results for the time development of ER. The conditions are the same as figure 1 except that $\nu = 0$. —·——·—, $Ri = 0.5$; – – – –, $Ri = 0.25$; ----------, $Ri = 0.088$.

energies and the fluxes depend on whether or not the flow is inviscid. Here $Pr = 1$. This differs from the case with no shear (Hanazaki & Hunt 1996). Without shear ($\alpha = 0$), the viscosity factor given by (4.16) reduces to $f_{\mathrm{vis}}(\theta_0, \phi_0) = 1/(1 + \nu t k_p^2)^{5/2}$ which is

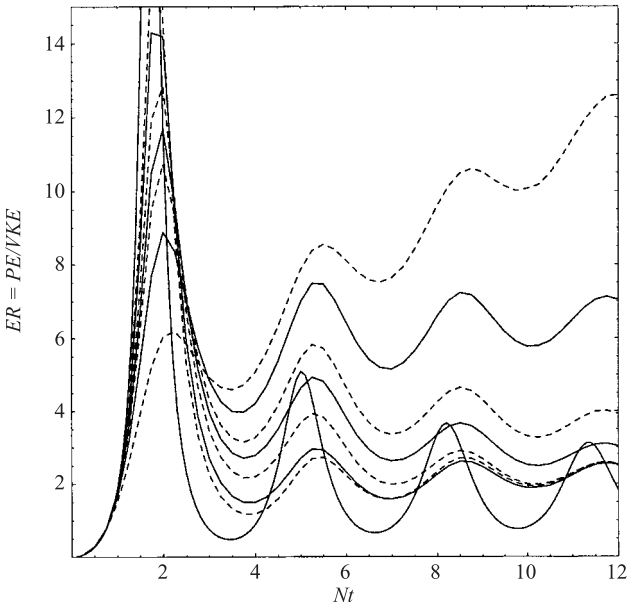

FIGURE 6. Time (Nt) development of the energy ratio $ER = PE/VKE$ for fixed $N(=2.729)$. The conditions are the same as figure 1 except that α varies according to $Ri = N^2/\alpha^2$ while N is fixed. At $Nt = 4$, from top to bottom, $Ri = 0.088$, 0.25, 0.4, 0.5, 0.66, 1.0, 1.32 and ∞. Dashed lines are used only to differentiate the neighbouring lines.

independent of θ_0 and ϕ_0, so that it is constant in the integrand of the variances and fluxes given by (4.13) to (4.15). Then the viscosity factor f_{vis} is cancelled out when we consider the 'ratios' of the energies and the fluxes, and the flow at $Pr = 1$ gives identical ratios as for the inviscid fluid, including ER and $\overline{\rho u_3}/(\overline{\rho^2}\,\overline{u_3^2})^{1/2}$. On the other hand, in shear flow, the viscosity effect has directional preference in the spectra as noted in § 4. Figure 7, which shows $\theta_0 - \phi_0$ distributions of the integrand for PE (integral B in (4.13)) and VKE (integral D in (4.14)), demonstrates that the distribution is more localized to $\phi = \pi/2$ and $3\pi/2$ in VKE than in PE, with smaller values away from $\phi_0 = \pi/2, 3\pi/2$. This explains why there are weaker effects of viscosity on VKE than on PE, and thence why there is a smaller $ER(=PE/VKE)$ in the viscous fluid. This localization also explains how the time oscillation of ER is maintained by a distinct oscillation of VKE near $\phi_0 = \pi/2, 3\pi/2$ (cf. § 3.2), while PE is almost monotonically decaying as shown in figure 2.

In figures 1 and 4, we notice that the oscillation period of the flux and energy ratios decreases with increasing Ri if we plot against αt. However, as shown in figures 6 and 8, the oscillation is actually determined by Nt (with period π/N), showing that the oscillation is controlled by stratification even in a shear flow. This has been previously noted in DNS by Holt *et al.* (1992, figure 21). What is interesting here is that, in the analytical forms of RDT solutions for the three-dimensional spectra or the fluxes, such as (3.12)–(3.14) and (3.20)–(3.22), time t appears in variable z only in the form of αt (cf. (3.3)), and Nt does not appear explicitly.

As already noted in § 3.2, the shear has no effect at $\cos\phi_0 = 0$, and the solution there is identical to the no-shear flow, which is determined only by Nt. Then, the oscillation of the spectra near $\cos\phi_0 = 0$ and its dominance is the reason why Nt becomes a

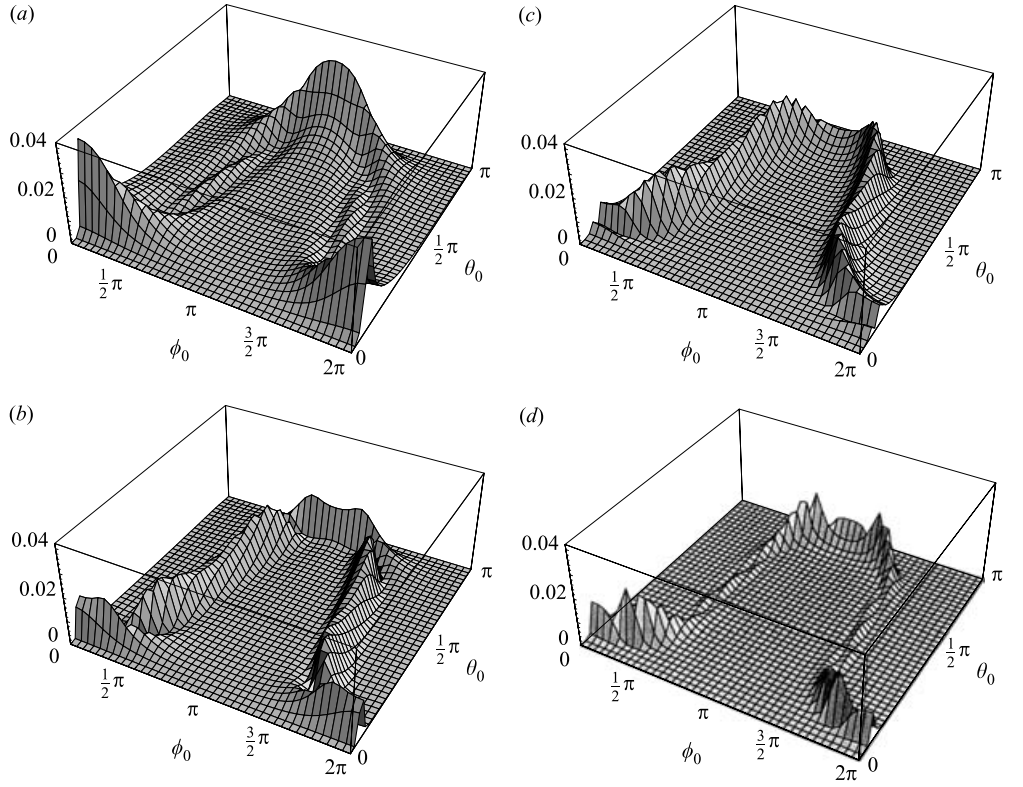

FIGURE 7. Integrand for the integrals B and D in (4.13) and (4.14), each of which gives the contribution of KE_0 to PE and KE respectively. $Ri = 1.32$, $N = 2.729$. Other conditions are the same as figure 1. (*a*) B ($Nt = 3.6$); (*b*) B ($Nt = 5.2$); (*c*) D ($Nt = 3.6$); (*d*) D ($Nt = 5.2$).

controlling parameter rather than αt, although in figures 6 and 8 comparison of the results with and without shear shows a small 'phase delay' due to the shear.

We notice from (4.10) that to isolate the effect of shear α, not only Nt but also νt must be identical, otherwise differences caused by viscosity obscure the result. In this study, comparisons are made for the same N, ν and t, i.e. for the same Nt and νt. For example in figures 6–8, we used fixed N and ν, while varying α to obtain different Ri. These conditions have not been considered in the previous DNS studies.

In figure 6, ER ($Nt \gg 1$) becomes almost independent of Ri (i.e. independent of shear) at large Ri ($\geqslant 0.66$), and in the limit of no shear ($Ri = \infty$), the ratio asymptotes to $ER = 3/2$ (Hanazaki & Hunt 1996). This is because at large $Ri(\geqslant 0.66)$, both VKE and PE increase for larger Ri (i.e. weaker shear), while at small $Ri(\leqslant 0.66)$, VKE increases but PE decreases for larger Ri so that ER decreases. On the other hand, when VKE and PE are plotted against αt, larger Ri (i.e. larger N) generally leads to smaller VKE and PE. This energy reduction occurs mainly at low wavenumbers (cf. figure 13).

Figure 7 shows the integrand for PE (cf. integral B in (4.13)) and VKE (cf. integral D in (4.14)) corresponding to the flow in figure 6 ($Ri = 1.32$). When ER takes a local minimum at $Nt = 3.6$, the integrand of PE (figure 7*a*,*b*) near $\phi_0 = \pi/2$ and $3\pi/2$ is nearly zero, while when ER takes a local maximum at $Nt = 5.2$ ($\sim 3.6 + \pi/2$) the components near $\phi_0 = \pi/2$ and $3\pi/2$ become large. On the other hand, the integrand

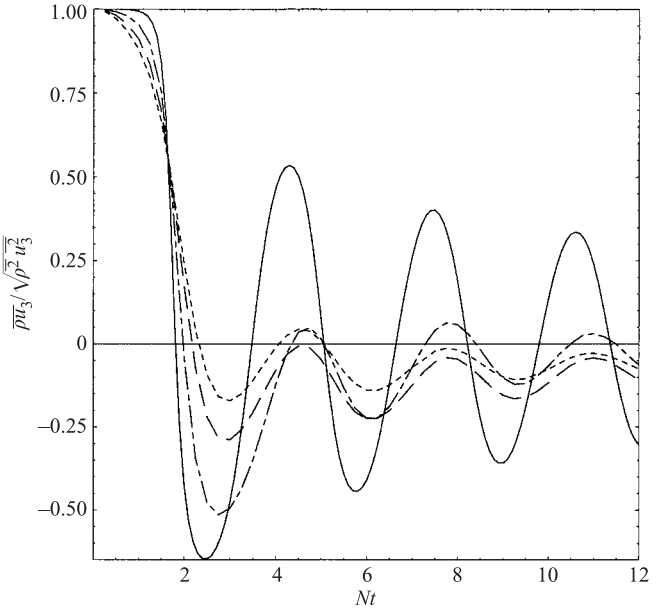

FIGURE 8. RDT results for the time development of the normalized vertical density flux for fixed $N(=2.729)$. The conditions are the same as figure 1 except that α varies according to $Ri = N^2/\alpha^2$ while N is fixed. ————, $Ri=\infty$; —·—·—, $Ri=1$; – – – –, $Ri=0.4$; ----------, $Ri=0.25$.

of *VKE* (figure 7*c*, *d*) oscillates in opposite phase to *PE*. This illustrates that the time oscillation of *ER* is due to the oscillation of the spectral components at $\phi_0 = \pi/2$, $3\pi/2$, where the solution is exclusively determined by the stratification, as noted in § 3.2.

This also explains the unsteady behaviour of the one-dimensional spectra in the experiments (Piccirillo & Van Atta 1997) similar to the RDT results given in figure 19) which shows that in the time interval when *ER* is increasing, $\Theta_{\rho\rho}(k_1)$ increases at low k_1 ($|\cos\phi_0| \ll 1$) due to stratification, while it decreases at high k_1 due to diffusion.

Figure 8 shows the time development of the normalized vertical density flux $\overline{\rho u_3}/(\overline{\rho^2}\,\overline{u_3^2})^{1/2}$ as a function of Nt for finite $Re \sim 43$. The oscillation period is equal to π/N, like *ER* (figure 6), and the results for $Ri = 0.25$ and 0.4 show a 'persistent' countergradient flux. We note that having smaller *Ri*, i.e. larger α, makes the earliest and the strongest countergradient flux weaker, showing that the shear reduces the countergradient flux. This is in agreement with the experiments by Komori & Nagata (1996) for $Ri = 0.4$, 1 and ∞, where the stronger shear with the same vertical temperature difference gave a weaker countergradient flux. We should note that, although the flux for no shear ($Ri = \infty$) gives large-amplitude oscillations, it oscillates in proportion to $\sim (Nt)^{-1/2}\sin(2Nt)$ long time (Hanazaki & Hunt 1996) so that the time-averaged value becomes zero. Then, when considering the time averaged value, the larger *Ri* does not necessarily give a stronger countergradient flux. In figure 8 ($0 \leqslant Nt \leqslant 12$), $Ri \sim 0.4$ gives the strongest 'persistent' countergradient flux.

Figure 9 shows the effect of initial energy ratio (ER_0) between the potential energy and the kinetic energy ($ER_0 = 0, \infty$) on the time development of normalized vertical density flux $\overline{\rho u_3}/(\overline{\rho^2}\,\overline{u_3^2})^{1/2}$. It shows that the flux oscillates in opposite phase for

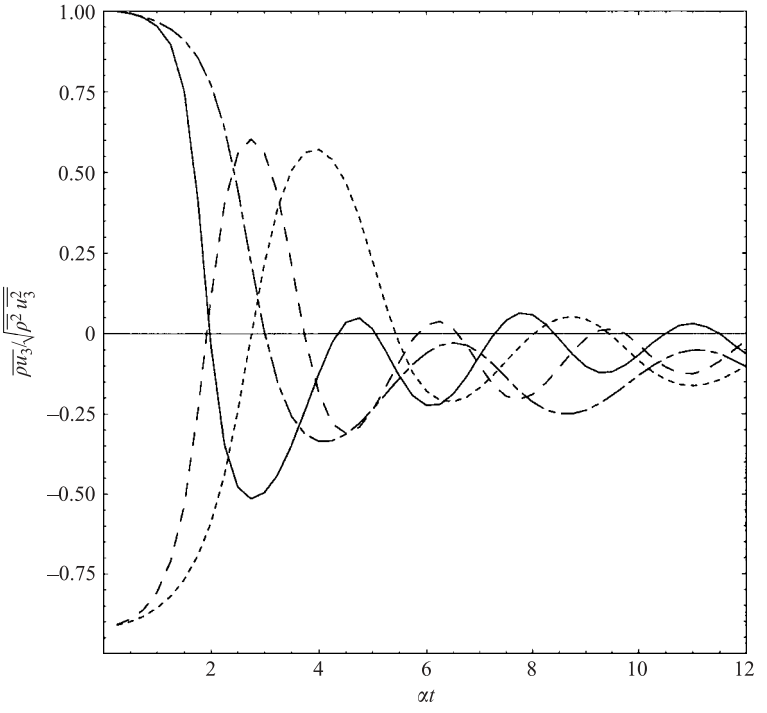

FIGURE 9. RDT results for the time development of the normalized vertical density flux for two initial conditions $PE_0 = 0 (ER_0 = 0)$ and $KE_0 = 0 (ER_0 = \infty)$ for $Ri = 0.5$ and 1.0. Other conditions are the same as figure 1. ————, $Ri = 1$, $PE_0 = 0$; —·——·—, $Ri = 0.5$, $PE_0 = 0$; – – – –, $Ri = 1$, $KE_0 = 0$; ----------, $Ri = 0.5$, $KE_0 = 0$.

$ER_0 = 0$ and ∞, but asymptotes to a value independent of $ER_0 (= 0, \infty)$ at long time. The initial values of $\overline{\rho u_3}/(\overline{\rho^2}\,\overline{u_3^2})^{1/2}$ agree with the prediction of the short-time approximation. For example, when $ER_0 = 0$, $\overline{\rho u_3}/(\overline{\rho^2}\,\overline{u_3^2})^{1/2} \to 1$ $(\alpha t \to 0)$ as already observed in figure 1, and when $ER_0 = \infty$, $\overline{\rho u_3}/(\overline{\rho^2}\,\overline{u_3^2})^{1/2} \to -\sqrt{5/6} = -0.913$ (cf. (3.32)). The flux for $Ri = 1$ shows that at larger Ri, i.e. with stronger stratification N, there is initially $(2 \leqslant \alpha t \leqslant 4)$ a stronger countergradient flux. But the mean value of the flux becomes more negative for $Ri = 0.5$ (smaller N) at long times, in agreement with figures 1 and 8. We have computed $\overline{\rho u_3}/(\overline{\rho^2}\,\overline{u_3^2})^{1/2}$ for other values of ER_0 which satisfy $ER_0 = Ri$, as has been investigated by Gerz *et al.* (1989), and confirmed good agreement. But the simultaneous change of ER_0 and Ri makes the interpretation complicated and we do not show those results here.

Figure 10 for ER also shows that the different initial energy ratios asymptote to the same value, although the tendency to asymptotic agreement is slow for $Ri = 0.25$. The final value of ER is determined by Ri here, but will depend also on the Prandtl number Pr since viscosity and diffusion will affect VKE and PE differently. Indeed, inviscid fluid generally gives larger values of ER as noted earlier in figure 5.

Previous DNS (Holt *et al.* 1992) have also shown that the long-time-limit values of the energy ratio ER $(\alpha t \gg 1)$ and the normalized flux $\overline{\rho u_3}/(\overline{\rho^2}\,\overline{u_3^2})^{1/2} (\alpha t \gg 1)$ are insensitive to the initial value of ER_0. At first sight, the insensitivity suggests the dominance of nonlinear effects, but our results show that it occurs in the linear framework.

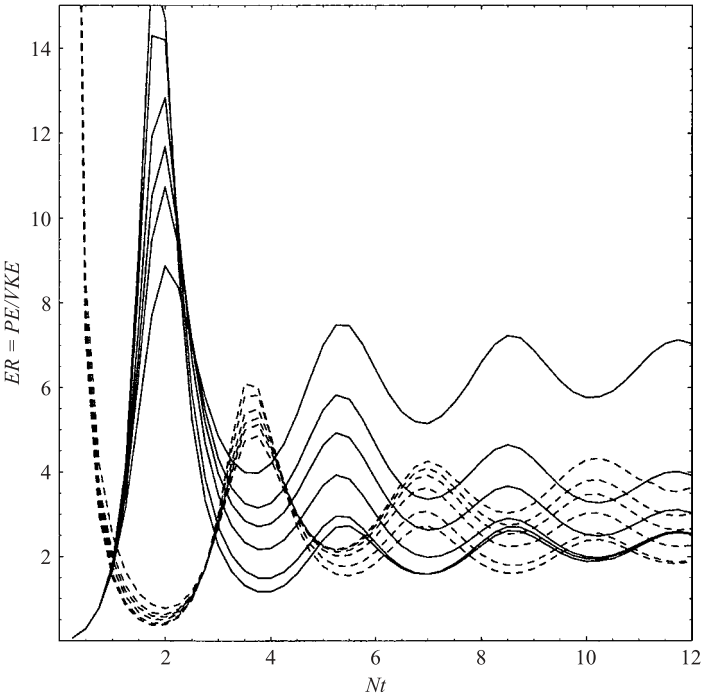

FIGURE 10. RDT results for the time (Nt) development of ER, for two initial conditions $PE_0 = 0$ ($ER_0 = 0$) and $KE_0 = 0 (ER_0 = \infty)$ but for fixed $N(= 2.729)$. The conditions are the same as figure 1 except that α varies according to $Ri = N^2/\alpha^2$. ————, $PE_0 = 0$; – – – –, $KE_0 = 0$. From top to bottom at $Nt = 5.5$, $Ri = 0.25$, 0.4, 0.5, 0.66, 1.0, 1.32.

To consider the reason why this occurs, we rewrite (4.13) to (4.15) in the following form:

$$PE = \frac{1}{2N^2}\overline{\rho^2} = \frac{1}{4\pi} PE_0 \times A(Ri, \alpha t) + \frac{Ri}{8\pi} KE_0 \times B(Ri, \alpha t), \tag{6.1}$$

$$VKE = \frac{1}{2}\overline{u_3^2} = \frac{1}{4\pi Ri} PE_0 \times C(Ri, \alpha t) + \frac{1}{8\pi} KE_0 \times D(Ri, \alpha t), \tag{6.2}$$

and

$$\overline{\rho u_3} = \alpha \left(\frac{1}{2\pi} PE_0 \times E(Ri, \alpha t) + \frac{Ri}{4\pi} KE_0 \times F(Ri, \alpha t) \right), \tag{6.3}$$

Where A to F denote the integrals in equations (4.13)–(4.15).

If $A \times D = B \times C$ or equivalently $A/B = C/D (= f(Ri))$ holds when $\alpha t \gg 1$, the energy ratio ER asymptotically becomes

$$ER(\alpha t \gg 1) = \frac{PE}{VKE} = \frac{B(Ri, \alpha t \gg 1)}{D(Ri, \alpha t \gg 1)} Ri = \frac{A(Ri, \alpha t \gg 1)}{C(Ri, \alpha t \gg 1)} Ri. \tag{6.4}$$

This shows clearly that ER ($\alpha t \gg 1$) is independent of the initial energy ratio $ER_0 = PE_0/VKE_0$ and depends only on the asymptotic ($\alpha t \gg 1$) ratios of the integrals which are determined by Ri. Physically the result $A/B = C/D (= f(Ri))$ shows that the ratios of the contributions from PE_0 and KE_0 are the same in PE and VKE, so that ER ($\alpha t \gg 1$) is independent of ER_0.

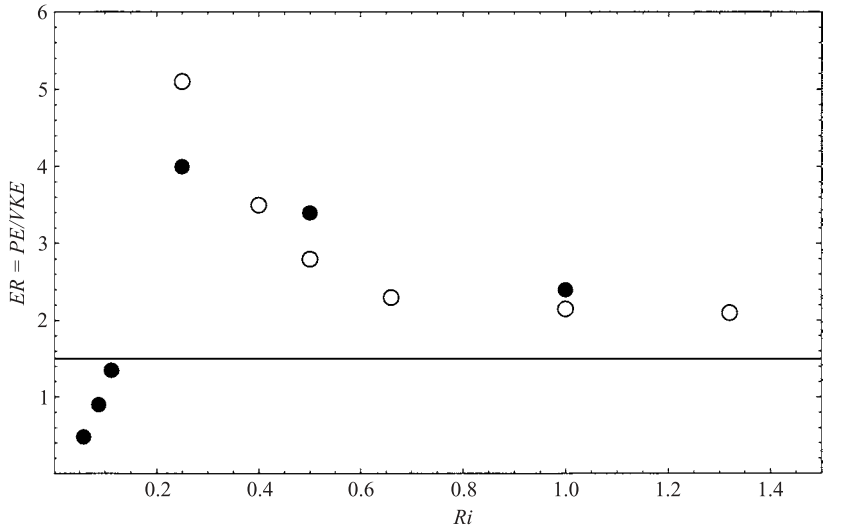

FIGURE 11. Richardson number dependence of the asymptotic value of ER ($Nt \to \infty$) when $Pr = 1$. Open circle denote the RDT results and the closed circle denote the DNS by Holt *et al.* (1992). The line at $ER = 3/2$ shows the RDT prediction for no-shear flow ($Ri = \infty$).

If, in addition, $B \times E = A \times F$ ($\alpha t \gg 1$) holds, then $A/B = C/D = E/F = f(Ri)$ ($\alpha t \gg 1$), indicating that

$$\frac{\overline{\rho u_3}}{\left(\overline{\rho^2}\,\overline{u_3^2}\right)^{1/2}}(\alpha t \gg 1) = \frac{F(Ri, \alpha t \gg 1)}{[B(Ri, \alpha t \gg 1)D(Ri, \alpha t \gg 1)]^{1/2}} = \frac{E(Ri, \alpha t \gg 1)}{[A(Ri, \alpha t \gg 1)C(Ri, \alpha t \gg 1)]^{1/2}}, \tag{6.5}$$

independent of ER_0. In the linear framework (RDT) numerical evaluation of integrals A to F indeed shows that the relation $A/B = C/D = E/F$ asymptotically holds at large times ($\alpha t \gg 1$). This is the reason why ER or $\overline{\rho u_3}/(\overline{\rho^2}\,\overline{u_3^2})^{1/2}$ is independent of the initial value ER_0.

The long-time-limit value of ER obtained numerically is given in figure 11, which shows that $ER(t \to \infty)$ is a decreasing function of Ri for $Ri \geqslant 0.25$. The dependence on Ri becomes weak for $Ri \geqslant 0.66$ but ER will decrease further as $Ri \to \infty$, since it will asymptote to 3/2 in the limit of $Ri = \infty$ (Hanazaki & Hunt 1996) as indicated by the straight line in the figure. The obtained values of $ER(Nt \to \infty)$ agree well with DNS by Holt *et al.* (1992) for $Ri \geqslant 0.25$, although the initial energy spectrum $E(k_0)$ is different. For small $Ri (< 0.25)$ where RDT results are not plotted, RDT significantly overestimates $ER(t \to \infty)$ as already noted in figures 4–6.

Figure 12 shows the time development of the one-dimensional co-spectrum $-\Theta_{\rho 3}(k_1)$ ($Ri = 0.5$) when it becomes countergradient (i.e. positive). The initial conditions are $PE_0 = 0$ and $E(k_0)$ is given by (4.9) as usually in experiments. Other parameters ν, α and k_p are chosen to agree with the experiments by Piccirillo & Van Atta (1997). At $\alpha t = 2.8$, $-\Theta_{\rho 3}(k_1)$ becomes countergradient, first at high wavenumbers. Since the solution of the RDT equations such as $-\Theta_{\rho 3}(k_1)$ contains αt in the form of $\alpha t k_1$, time t is always coupled with k_1. In addition, in the variable $z_0 = \mathrm{i}(r \sin\varphi + \alpha t k_1)/(k_1^2 + r^2 \cos^2\varphi)^{1/2}$ (cf. (5.5)) which determines the time oscillation, $\alpha t k_1/(k_1^2 + r^2 \cos^2\varphi)^{1/2}$ increases monotonically with k_1. Then, the increase of k_1 and of t has a similar effect.

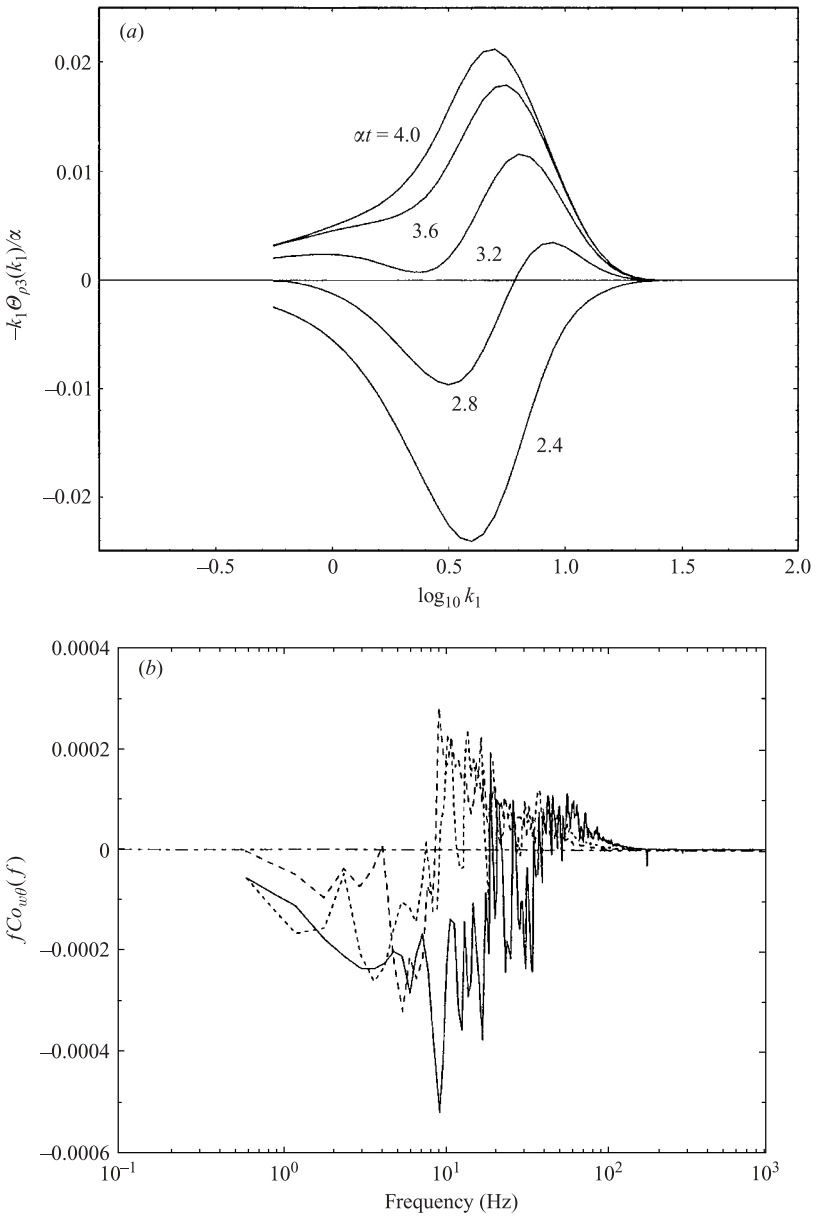

FIGURE 12. Time development of the one-dimensional cospectrum $-k_1\Theta_{\rho 3}(k_1)/\alpha$ for $Ri = 0.5$. The conditions are similar to the experiments by Piccirillo & Van Atta (1997) except for the Prandtl number ($Pr = 1$) and that $E(k_0)$ is given by (4.9). In the experiments, $U = 220\,\mathrm{cm\,s^{-1}}$, peak frequency $f = 10\,\mathrm{s^{-1}}$, $\nu = 0.15\,\mathrm{cm^2\,s^{-1}}$, $\alpha = 3.35\,\mathrm{s^{-1}}$, but non-dimensionalization by length scale $l = 2\pi/220\,\mathrm{cm}$ is used here so that peak wavenumber becomes $k_p = 10$ instead of $2\pi f/U\,\mathrm{cm^{-1}}$. From bottom to top, each line corresponds to $\alpha t = 2.4$, 2.8, 3.2, 3.6 and 4.0 respectively. (*a*) RDT, (*b*) experiments by Piccirillo & Van Atta (1997).

This explains why the countergradient spectra occur sooner at high wavenumbers and agrees with the stratified shear flow experiments for high ($Pr = 6600$: Komori & Nagata 1996) and low Prandtl numbers ($Pr = 0.7$: Piccirillo & Van Atta 1997).

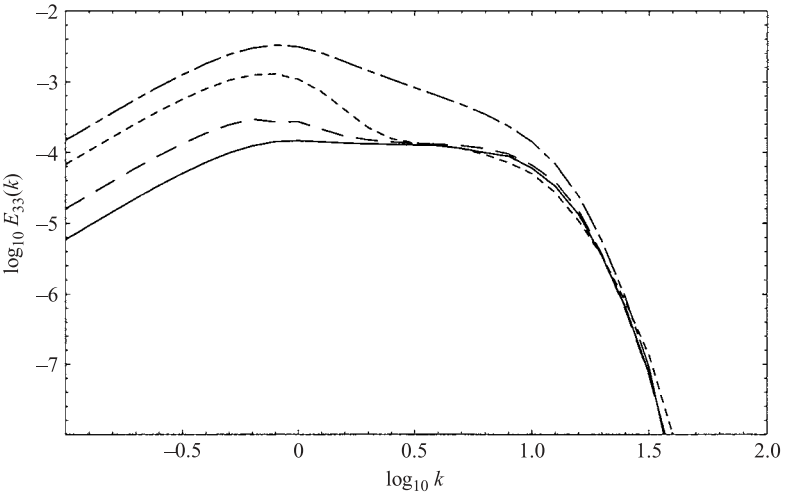

FIGURE 13. Three-dimensional radial spectra $E_{33}(k)$ at $\alpha t = 20$ for various Ri. $Pr = 1$, $E(k_0)$ given by (4.9), $k_p = 20$, $\nu = 0.01$, $\alpha = 20\sqrt{2}$. The conditions are similar to DNS by Holt *et al.* (1992) except the functional form of $E(k_0)$. — - — - —, $Ri = 0$; --------, $Ri = 0.088$; – – – –, $Ri = 0.25$; ————, $Ri = 1$.

This is in contrast to the no-shear flow, where $Pr = 0.7(< 1)$ gives low-k_1 countergradient flux (Lienhard & Van Atta 1990; Yoon & Warhaft 1990) while $Pr = 6(> 1)$ gives high-k_1 countergradient flux (Komori & Nagata 1996). The RDT result for no-shear flow (Hanazaki & Hunt 1996) shows this difference due to the Prandtl number, but it gives high-k_1 countergradient flux in the one-dimensional spectra also for $Pr = 1$ and inviscid fluid. Therefore, we should be cautious about the Prandtl number dependence in the one-dimensional spectra and further investigations are needed on the effect of the Prandtl number ($Pr \neq 1$) in shear flow.

Figure 13 shows the radial spectra of the vertical kinetic energy $E_{33}(k)$ (cf. (5.7)) at large time ($\alpha t = 20$), under the same conditions as Holt *et al.* (1992) except the initial spectral form. In general the effect of stratification is more significant at low wavenumbers as conjectured by Hunt *et al.* (1988) in their length-scale analysis. With the increase of Ri (or N), a flat spectrum ($\propto k^0$) appears for $1 \leqslant k \leqslant 10$. The flat spectrum can be observed also in the DNS results by Holt *et al.* (1992, see their figure 9) for $Ri = 0.088$, although RDT results may not be applied to the linearly unstable cases where $Ri < 0.25$.

When there is no stratification ($Ri = 0$), the asymptotic spectrum gives a region of $E_{33}(k) \propto k^{-1}$ power spectrum at $1 \leqslant k \leqslant 10$. This can be verified by noting that the main contribution to the integral representation of $E_{33}(k)$ comes from near $\theta(t) = \pi/2$ and $\phi = \pi/2, 3\pi/2$ (see also figure 14*c*) in the initial energy spectrum $E(k_0)$, as already discussed at the end of § 5. The asymptotic analysis ($\alpha t \gg 1$) for $E_{33}(k)$ with $Ri = 0$, i.e. for

$$E_{33}(k) = \frac{1}{8\pi} \int_0^{\pi} \mathrm{d}\theta \int_0^{2\pi} \mathrm{d}\phi \sin^3\theta E\left(k[\sin^2\theta + (\cos\theta + \alpha t \sin\theta\cos\phi)^2]^{1/2}\right) \times \exp\left(-2\nu t k^2 \left(1 + \alpha t \sin\theta\cos\theta\cos\phi + \frac{1}{3}(\alpha t)^2 \sin^2\theta\cos^2\phi\right)\right), \quad (6.6)$$

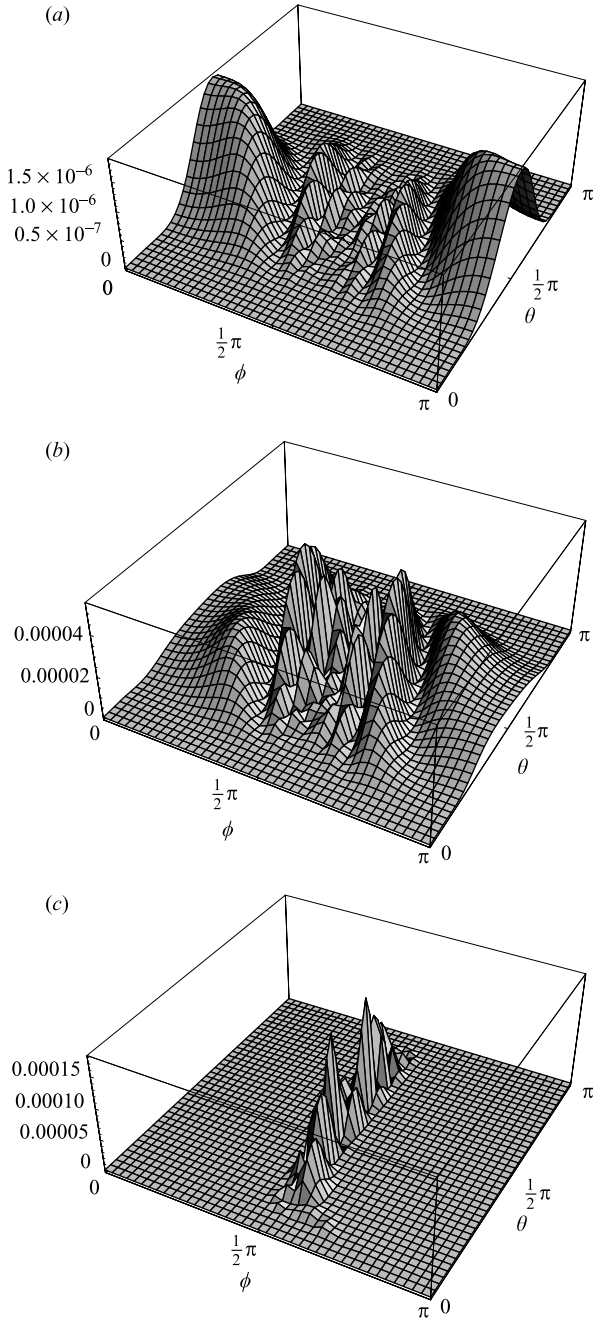

FIGURE 14. Integrand of $E_{33}(k)$ at $\alpha t = 20$ and $Ri = 1$ for various wavenumbers. Conditions are the same as figure 13. (*a*) $k = 10^{-1}$; (*b*) $k = 1$; (*c*) $k = 10$.

shows that the vertical velocity spectrum asymptotically ($\alpha t \gg 1$) has the form

$$E_{33}(k) \sim \frac{2KE_0}{\alpha t k} \left(\frac{k_p}{\alpha t} \ll k \ll k_p \right). \tag{6.7}$$

Here, the peak wavenumber k_p is comparable with the inverse of the energy-containing scale l_0 or the integral scale L_X ($k_p \sim l_0^{-1} \sim L_X^{-1}$). Other initial spectra such as (4.11) lead to the same k^{-1} spectrum independent of the viscosity. This illustrates, and we can also verify analytically, that the low-wavenumber power spectrum of the form $\propto k^{-1}$ is independent of the initial spectrum as long as initially it has the form of $E(k_0) \propto k_0^{2n}$ ($n \geqslant 1$) at low wavenumbers ($k_0 \ll k_p$).

Since the lower bound for k is given by $k_p/(\alpha t)$ in (6.7), the k^{-1} spectrum extends to progressively lower wavenumbers with time αt. This could be verified by the numerical results, although the time development is not shown here.

In a study of the high-wavenumber spectrum ($k_p \ll k \ll (\alpha t)k_p$) in unstratified shear flows (Hunt & Carruthers 1990), assuming significant nonlinear effects at low wavenumbers where much energy resides, the initial spectrum of the form $E(k_0) \propto \exp(-k_0^2/k_p^2)$ has been used and it asymptotically gave $E_{33}(k) \propto k^{-4}$. In contrast the present results show that the k^{-1} spectrum reflects the characteristics of turbulence at lower wavenumbers. Further studies of these general asymptotic properties of spectra are needed.

The effect of stratification N is clearly observed at low wavenumbers ($k \leqslant 1$), where a significant decrease of vertical kinetic energy due to large N (or Ri) is observed. Therefore, when VKE is plotted against αt, larger N (i.e. Ri) gives smaller VKE as noted earlier (see the discussion of figure 6). Thus the decay of VKE is faster for larger N. In the very low-wavenumber region ($k \leqslant 1$), $E_{33}(k) \propto k^2$ holds for all Ri since (4.9) gives $E(k_0) \propto k_0^2 (k_0 \ll k_p)$ there so that $E(k_0) = E(k(\sin^2\theta + (\cos\theta + \alpha t \sin\theta\cos\phi)^2)^{1/2}) \propto k^2(\sin^2\theta + (\cos\theta + \alpha t \sin\theta\cos\phi)^2)$ ($k \ll k_p$) and the factor k^2 is cancelled in $\Phi_{33}(\boldsymbol{k}, t)_{\text{inv}}$, which is given by (5.9). In addition, the viscosity effects contained in Φ_{33} (cf. (5.8)) are negligible when $\nu t k^2 \ll 1$ is satisfied. Therefore, Φ_{33} is independent of k at low wavenumbers, and (5.7) gives $E_{33}(k) \propto k^2$ if both $\nu t k^2 \ll 1$ and $k \ll k_p$ are satisfied. In the present case, at $\alpha t = 20$ these conditions become $k \ll 1/(\nu t)^{1/2} \sim 12$ and $k \ll k_p = 20$, consistent with the numerical results, i.e. $k \leqslant 1$.

On the other hand, at high wavenumbers ($k \geqslant 10^{0.5}$), the results for $Ri > 0$ (i.e. $N \neq 0$) give almost the same spectra, suggesting that the effect of stratification N ($\neq 0$) is not important. However, over a long time ($\alpha t \gg 1$), comparison with the spectrum for unstratified flow ($Ri = 0$) shows that even a weak stratification gives a significant reduction of $E_{33}(k)$. At large times dominant contributions to $E_{33}(k)$ (for $k \geqslant 10^{0.5}$) come from near $\phi = \pi/2, 3\pi/2$ (see the end of § 5 and figure 14*c*) where the behaviour is determined only by stratification N. The three-dimensional spectrum is given by

$$\Phi_{33}(\boldsymbol{k}, t)_{\text{inv}} = \frac{\sin^2\theta}{4\pi k^2}(1 - \cos(2Nt\sin\theta))S(k) + \frac{\sin^2\theta}{8\pi k^2}(1 + \cos(2Nt\sin\theta))E(k) \quad (\phi = \pi/2, 3\pi/2). \tag{6.8}$$

This shows that the integrand at $\phi = \pi/2$ oscillates in the θ-direction with wavelength $\theta = \sin^{-1}[\pi/(Nt)] = \sin^{-1}[\pi/(Ri^{1/2}\alpha t)]$. Thus if αt is the same, Nt is larger for larger Ri, giving a smaller wavelength in the θ-direction. However, the contribution to the energy of the oscillating part diminishes $\propto (Nt)^{-1/2}$ with the application of the method of steepest descents (Hanazaki & Hunt 1996). On the other hand, the steady part of (6.8) is independent of $N(\neq 0)$ (or $Ri(\neq 0)$) and only this steady part contributes to $E_{33}(k)$ at large times ($\alpha t \gg 1$ or more precisely $Nt > O(1)$), which is

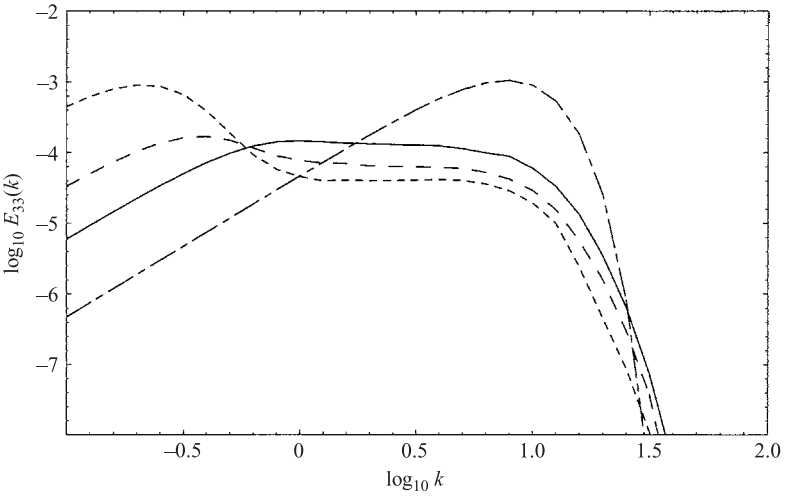

FIGURE 15. Three-dimensional radial spectra $E_{33}(k)$ at $Nt = 20$ for various Ri. The conditions are the same as figure 13 except that α varies according to $Ri = N^2/\alpha^2$ while $N(=20\sqrt{2})$ is fixed. --------, $Ri = 0.088$; – – – –, $Ri = 0.25$; ————, $Ri = 1$; — - — - —, $Ri = \infty$ (no shear).

given by

$$\frac{\sin^2\theta}{8\pi k^2}(E(k) + 2S(k)) \quad (N, Ri \neq 0, \alpha t \gg 1, |\cos\phi| \ll 1). \tag{6.9}$$

This is the reason why different Ri or N ($\neq 0$) gives almost the same $E_{33}(k)$ at high wavenumbers. Indeed larger αt (i.e. Nt) gives better agreement for different $Ri(\neq 0)$.

When there is no stratification ($N = Ri = 0$), $\Phi_{33}(k)$ becomes

$$\Phi_{33}(\mathbf{k}, t)_{\text{inv}} = \frac{\sin^2\theta}{4\pi k^2}E(k) \quad (N = Ri = 0, |\cos\phi| \ll 1), \tag{6.10}$$

because $\cos(2Nt\sin\theta) = 1$. Then, if either $E(k) > 2S(k)$ or equivalently $KE_0 > 2PE_0$ is satisfied, comparison of (6.10) with (6.9) shows that $E_{33}(k)(Ri > 0) < E_{33}(k)(Ri = 0)$ holds at large times ($Nt > O(1)$) and the vertical kinetic energy reduces. For example, if $PE_0 = 0$ (or $S(k) = 0$) as in the present case, even a weak stratification will halve the value of $E_{33}(k)$, but the reduced value is independent of the strength of stratification $N(\neq 0)$. The above explanations are not exact but explain qualitatively most of the results obtained.

To see the effect of purely the shear α, $E_{33}(k)$ for the same N, ν and t ($Nt = 20$) is shown in figure 15. The results for $Ri = 1 (N = \alpha)$ are the same as figure 13. Stronger shear (smaller Ri) gives larger $E_{33}(k)$ at low wavenumbers ($k \leqslant 1$) and smaller $E_{33}(k)$ at high wavenumbers ($k \geqslant 1$), i.e. the shear significantly enhances the large-scale vertical motion while inhibiting the small-scale vertical motion. When $E_{33}(k)$ is integrated, smaller Ri (larger α) gives faster decay of VKE (cf. figure 6), showing that the high-wavenumber decay overcomes the low-wavenumber increase, although the high-wavenumber components at $Ri = 0.088 < 0.25$ would be underestimated in RDT as noted in figure 2.

The time development of $E_{33}(k)$, (not shown here), shows that the bandwidth of the flat spectrum, i.e. $10^{-0.2} \leqslant k \leqslant 10^{1}$, is determined by Nt, being elongated to the low-wavenumber region with time. This is independent of Ri (or α), showing that

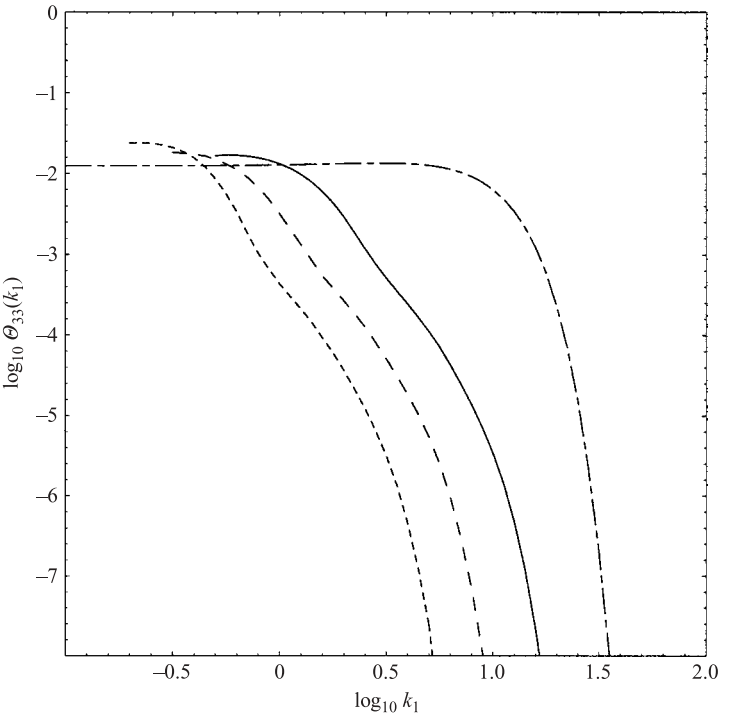

FIGURE 16. One-dimensional spectrum $\Theta_{33}(k_1)$ at $Nt = 10$ for various Ri. The conditions are the same as figure 12, i.e. similar to the experiments by Piccirillo & Van Atta (1997) except for the Prandtl number ($Pr = 1$) and that $E(k_0)$ is given by (4.9). --------, $Ri = 0.088$; – – – –, $Ri = 0.25$; ————, $Ri = 1$; — - — - —, $Ri = \infty$ (no shear).

its appearance is governed by stratification. We should note, however, that the flat spectrum does not appear when there is no shear ($Ri = \infty$), showing that both the shear and the stratification are necessary for the generation of the flat spectrum (or the blocking effect of a rigid surface (Hunt & Carlotti 2001).

It is of interest to note that at high wavenumbers both the shear and the stratification work to reduce $E_{33}(k)$ and $E_{\rho\rho}(k)$. This means that even if Ri is the same, larger α and N reduce the high-wavenumber components. This is consistent with the fact that the linear approximation becomes a better approximation for larger α and N (cf. figure 1).

For comparison with the experiments we need to investigate the one-dimensional spectra $\Theta_{33}(k_1)$. Figure 16 shows that the shear reduces the high-horizontal-wavenumber components, i.e. the turbulent structure becomes longer in the x_1-direction consistent with the generation of the streaks. This can be explained by the fact that for large k_1, viscous effects are large, particularly at large αt as is clear in (5.2).

The radial spectra of the potential energy given in figure 17 ($\alpha t = 20$) show that stratification generally reduces the potential energy at all scales, in contrast to $E_{33}(k)$ (figure 13) which showed insensitivity to $N(\neq 0)$ at high wavenumbers. The difference appears since the non-zero region of the integrand is not localized to $\phi = \pi/2, 3\pi/2$ in $E_{\rho\rho}(k)$ compared to $E_{33}(k)$. A nearly flat spectrum region ($10^0 \leqslant k \leqslant 10^1$) appears at large times ($\alpha t = 20$) which would correspond to $E_{33}(k)$ (figure 13). The flat spectrum in $E_{\rho\rho}$ has been observed also in DNS by Kaltenbach *et al.* (1994, their figure 13*b*).

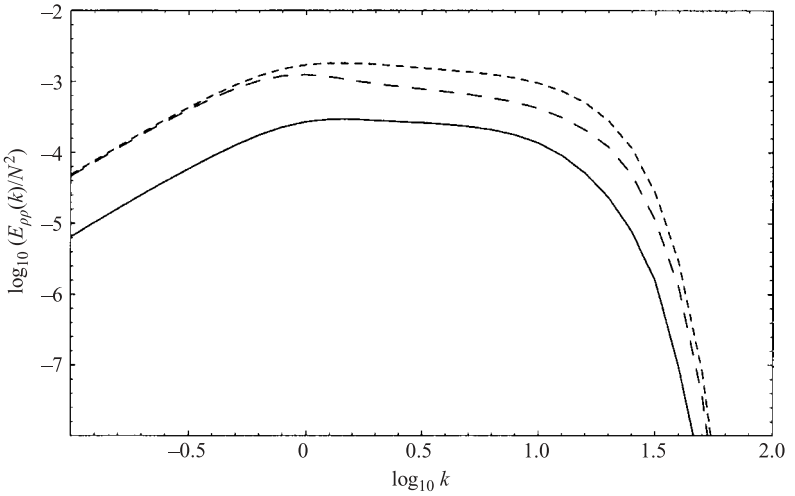

FIGURE 17. Three-dimensional radial spectra $E_{\rho\rho}(k)$ at $\alpha t = 20$ for various Ri. The conditions are the same as figure 13. --------, $Ri = 0.088$; – – – –, $Ri = 0.25$; ————, $Ri = 1$.

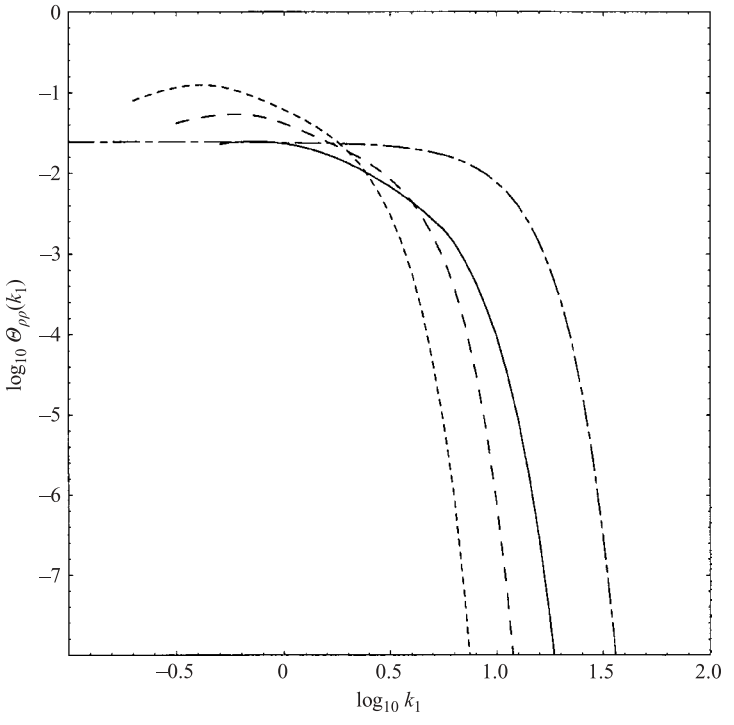

FIGURE 18. One-dimensional spectrum $\Theta_{\rho\rho}(k_1)$ at $Nt = 10$ for various Ri. The conditions are the same as figures 12 and 16 except that $N = 3.35\,\mathrm{s}^{-1}$ is fixed while α is varied with Ri. --------, $Ri = 0.088$; – – – –, $Ri = 0.25$; ————, $Ri = 1$; — - — - —, $Ri = \infty$ (no shear).

The one-dimensional potential energy spectrum $\Theta_{\rho\rho}(k_1)$ at $Nt = 10$ given in figure 18 shows that the shear (smaller Ri) gives smaller high-wavenumber energy, which is similar to the behaviour of $\Theta_{33}(k_1)$. We also notice that a spectrum proportional to $k^{-1.2}$ appears at $10^{-0.3} \leqslant k_1 \leqslant 10^{0.8}$ particularly at low Ri. Rohr *et al.* (1988, their

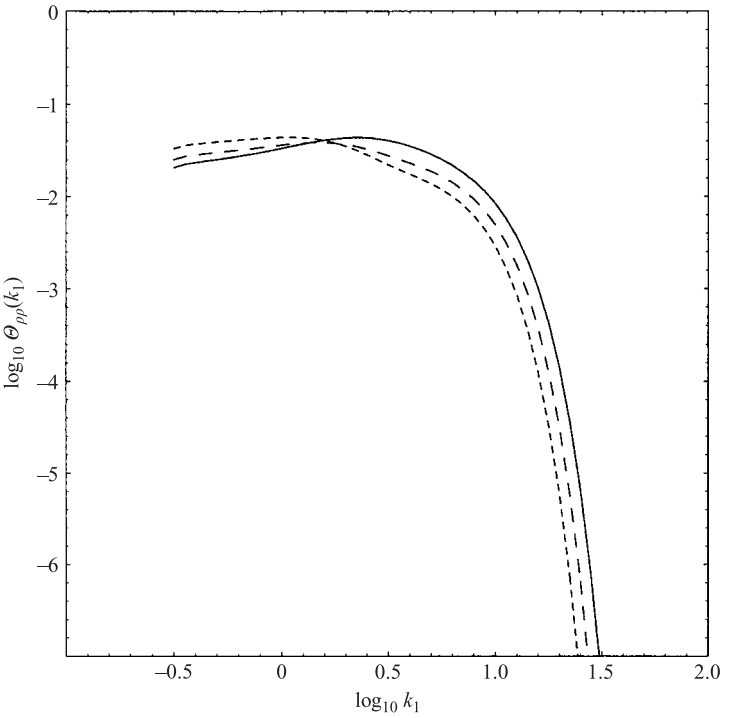

FIGURE 19. Time development of the one-dimensional spectrum $\Theta_{\rho\rho}(k_1)$ for $Ri = 0.44$. The conditions are the same as figure 12 and 16 with similarity to the experiments by Piccirillo & Van Atta (1997). ———, $\alpha t = 4.87$; – – – –, $\alpha t = 6.38$; - - - - - - - -, $\alpha t = 7.54$.

figure 23*a*) found a similar spectrum and argued that $\Theta_{\rho\rho}(k_1) \propto k^{-1.2}$ observed in thermally stratified water flow ($Pr \gg 1$) is consistent with the fact that the viscous subrange lies between the $k^{-5/3}$ (inertial) and k^{-1} (viscous–convective) subrange, which has also been observed by Gibson & Schwarz (1963). They attributed the significant attenuation in the high-wavenumber region to the resolution of the probe. However, in this study, similar spectra appeared even with $Pr = 1$ and so the same explanation cannot be applied here, and another explanation becomes necessary. Since the power spectra appear more clearly at low Ri (larger α), the spectrum is associated with the shear. Similar spectra ($\propto k^{-1.2}$) can be found in the LES results by Kaltenbach *et al.* (1994, figure 13*d*) for $Pr = 1$. Note also that the vertical power spectrum for the vertical kinetic energy (figure 16) shows that $\Theta_{33}(k_1) \propto k_1^{-4}$ in the same wavenumber region.

The time development of $\Theta_{\rho\rho}(k_1)$ for $Ri = 0.44$ ($4.87 \leqslant \alpha t \leqslant 7.54$) is shown in figure 19 for comparison with the experiments by Piccirillo & Van Atta (1997). The total potential energy PE decreases for $\alpha t \geqslant 2.5$ in RDT as is expected from figure 2, but the monotonic decay occurs only at high wavenumbers since the low-wavenumber components oscillate with time. When the low-wavenumber components are increasing, the peak wavenumber decreases with time in agreement with the experiments by Piccirillo & Van Atta (1997, figure 14). Indeed when $Ri = 0.44$, ER is increasing for $5 \leqslant \alpha t \leqslant 7.5$ (cf. figure 4, $Ri = 0.5$). The integrand of B (PE) is increasing near $\cos\phi_0 = 0$ ($k_1 = 0$), similar to figures 7(*a*) and 7(*b*). Then $\Theta_{\rho\rho}(k_1)$ increases at low k_1, while it decreases elsewhere due to the shear and the diffusion, so that PE generally decreases with time. The main difference between RDT and the experiments is that in RDT, high-wavenumber components decrease monotonically with time even

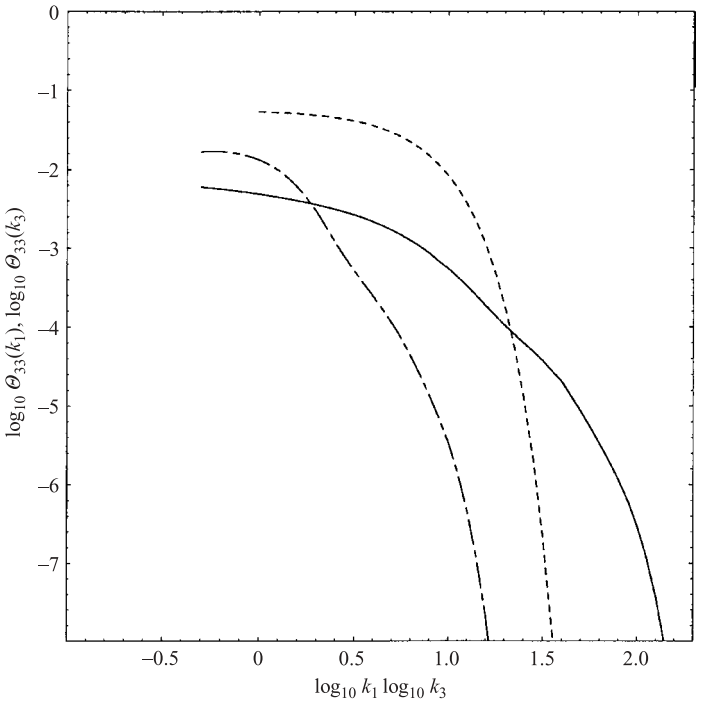

FIGURE 20. Vertical and horizontal spectrum $\Theta_{33}(k_3)$ and $\Theta_{33}(k_1)$ at $Nt = 10$ ($Ri = 1$). The conditions are the same as figure 12. - - - - - - - -, $\Theta_{33}(k_3)$ (and $\Theta_{33}(k_1)$) at $Nt = 0$; — - — - —, $\Theta_{33}(k_3)$ ($Nt = 10$); ————,$\Theta_{33}(k_1)$ ($Nt = 10$).

when $Ri < 0.25$, and the increase of the potential energy PE is suppressed, while in the experiments for $Ri = 0.04$ high-wavenumber spectra become steady so that PE increases with time. This suggests that the absence of nonlinear interaction in RDT means that the energy of the high-wavenumber components is underpredicted. This leads to an underprediction of the potential energy.

To see the vertical spectrum, which is often observed in the ocean, we show $\Theta_{33}(k_3)$ along with $\Theta_{33}(k_1)$ in figure 20. Initially, at $Nt = 0$, $\Theta_{33}(k_3)$ and $\Theta_{33}(k_1)$ agree because of the initial isotropy assumed here, but as time elapses the vertical spectrum has progressively more energy at small scales (i.e. high k_3), while the horizontal spectrum has more energy at large scales (i.e. low k_1). As observed in figure 15, shear generally reduces the high-$k(=|\boldsymbol{k}|)$ components, but the vertical spectrum behaves differently. This can be understood by the analytical form of the vertical spectrum. If we use the cylindrical coordinates with $k_1 = k_H \cos\phi$, $k_2 = k_H \sin\phi$ and $k_3 = k_{30} - \alpha t k_1$, we can write $\Theta_{33}(k_3)$ as

$$\begin{aligned}\Theta_{33}(k_3) &= \int_0^\infty \mathrm{d}k_H k_H \int_0^{2\pi} \mathrm{d}\phi \Phi_{33}(\boldsymbol{k}, t) \\ &= \frac{1}{2\pi} \int_0^\infty \mathrm{d}k_H \\ &\quad \times \int_0^\pi \mathrm{d}\phi \frac{1}{k_H} \left| P_\nu'(z) Q_\nu(z_0) - P_\nu(z_0) Q_\nu'(z) \right|^2 E\left(\left[k_H^2 + (k_3 + k_H \alpha t \cos\phi)^2 \right]^{1/2} \right) \\ &\quad \times \exp\left(-2\nu t \left(k_H^2 + k_3^2 + k_H k_3 \alpha t \cos\phi + \frac{1}{3} k_H^2 (\alpha t \cos\phi)^2 \right) \right), \end{aligned} \tag{6.11}$$

where ν is given by (5.11), and

$$z = \mathrm{i}\frac{k_3}{k_H}, \quad z_0 = \mathrm{i}\left(\frac{k_3}{k_H} + \alpha t \cos\phi\right). \tag{6.12}$$

The form of $E(k_0) = E([k_H^2 + (k_3 + k_H \alpha t \cos\phi)^2]^{1/2})$ in (6.11) shows that at large times ($\alpha t \gg 1$), if $k_1 = k_H \cos\phi < 0$, $E(k_0)$ takes the initial value at $t = 0$ for larger values of $k_3 (\gg k_{30})$, giving more energy at higher wavenumbers. In particular, at very large vertical wavenumber $k_3/(\alpha t) \gg 1$, components of $\cos\phi = -1$ (i.e. $\phi = \pi$) become dominant.

Since this discussion is related only to the shear and not to the stratification, the difference between the horizontal and vertical spectrum will be the same in general shear flow with or without stratification. The results should be similar also for other velocity components and potential energy. Indeed, numerical RDT results for Θ_{11} and $\Theta_{\rho\rho}$ also showed a similar difference. In previous RDT for unstratified shear flow Hunt & Carruthers (1990) showed similar results for Θ_{11}, and in a recent experiment on the density spectra $\Theta_{\rho\rho}$, Keller & Van Atta (2000) also showed similar results.

7. Conclusions

In this study, we have investigated some of the main mechanisms governing stratified turbulence with vertical shear using the linear rapid distortion theory (RDT) for homogeneous flows developing with time. The analytical solutions of RDT equations are found to be described by Legendre functions of complex degree with pure-imaginary argument. The numerical evaluation of the analytical results showed good agreement with DNS for stable mean flow ($Ri \geqslant 0.25$) particularly at low turbulent Froude numbers or at high shear numbers when the nonlinear effects are less significant. Some significant effects depend on nonlinear processes and are clearly not modelled by RDT, particularly at very low values of Ri.

Initially, as turbulence develops, many of the characteristics are, as experiments indicate, similar to those in unsheared flow, since at leading order the energy and the fluxes are determined by Nt, and the effect of shear usually appear at higher order.

The countergradient density and momentum fluxes also occur with shear ($Ri \leqslant 1.0$), and are described by the linear theory. However, when Ri is above a critical value of $Ri_{crit} \sim 0.3$, these fluxes oscillate with time coherently across the whole flow. Also, the mean values of these fluxes decrease and approach zero as Ri increases. This structural change in the sheared turbulence appears to be the main mechanism for its suppression by stable stratification.

The ratio $ER(=PE/VKE)$ (for large $\alpha t \gg 1$, $Nt \gg 1$) of the potential energy to the vertical kinetic energy generally decreases with $Ri(\geqslant 0.25)$, reaching the smallest value of 3/2 when there is no shear ($Ri = \infty$), although for $Ri \geqslant 0.5$ the variation is less than 30%. Thus there is good agreement with the previous DNS for $Ri \geqslant 0.25$. But when $Ri < 0.25$, the turbulent energy and ER grow with time because RDT estimates $\overline{u_3^2}$ incorrectly. Although the linear theory is inappropriate in this range (for this velocity component and for ER), it does indicate that in a uniform shear flow the turbulence structure undergoes a critical transformation when $Ri \sim 0.3$, as the DNS results of Gerz & Schumann have shown.

This result is reasonably robust, as we see that both the energy ratio ER and the normalized vertical density flux $\overline{\rho u_3}/(\overline{\rho^2}\,\overline{u_3^2})^{1/2}$ are independent of the initial value ER_0, and are also primarily determined by linear processes even with shear.

In the radial and horizontal spectra, stratification governs the buoyancy oscillation in the vertical plane (θ-direction) while the shear determines the localization in the ϕ-direction to $\phi \to \pi/2, 3\pi/2$ (or $k_1 \to 0$) in the (θ, ϕ) space (cf. (2.7)) The localization with time is mainly due to the spectral deformation given by $E(k_0) = E((k_1^2 + k_2^2 + (k_3 + \alpha t k_1)^2)^{1/2})$, where k_0 is the initial radial wavenumber. This means that for the vertical wavenumber spectrum, the main contribution for high k_3 comes from the negative value of k_1/k_3 and negative $\cos\phi$ ($\phi \sim \pi$) (i.e. small values of $k_2/k_1 = \tan\phi$). The amplitudes of these spectra grow with time. By contrast, for the radial and horizontal components (k, k_1), the high-wavenumber components decrease quite rapidly. These spectral forms are affected more by shear than by stratification. So stratified and unstratified shear flows should have the same high-wavenumber spectra away from the boundaries, as indeed tends to be observed.

The effect of shear on viscous decay is not significantly affected by stratification and is identical to that in pure shear flow, i.e. the components of larger streamwise wavenumber k_1 decay faster, leaving the components of smaller k_1. In combination with the effect of spectrum deformation, the energy and the flux are increasingly dominated by the small-k_1 components as time elapses. Since the components of $k_1 = 0$ are unaffected by the shear and oscillate in time with period π/N, this explains why the energies and the fluxes oscillate at period π/N even in a shear flow.

The contribution of long streamwise eddies ($k_1 = 0$) explains many of the spectral behaviours. For example, the radial spectra of the vertical kinetic energy $E_{33}(k)$ at large times are almost independent of the stratification $N(\neq 0)$ at high wavenumbers, since only the steady components contribute to $E_{33}(k)$. But we note that even a weak stratification reduces $E_{33}(k)$ at small scales if $KE_0 > 2PE_0$ due to the decrease of quasi-steady components. The inviscid stratification effect on the decrease of VKE is generally more significant at large scales, in agreement with the conjectures by Hunt *et al.* (1988).

The effect of stratification N and shear α at high wavenumbers (k or k_1) is to reduce both VKE and PE. Even for the same Ri, larger N and α would reduce the high-wavenumber components of VKE and PE. This is consistent with the assumption of linearity of the governing equations justified for large N and α. It leads to smaller VKE and PE at small scales. On the other hand, at small k, the effects of stratification and shear oppose each other, i.e. VKE and PE decrease due to the stratification but increase due to the shear. Then, when the spectrum is integrated, both VKE and PE decay faster for larger N. But the dependence on α is more complicated. The VKE decays faster for larger α, but the dependence of PE on α is not monotonic, giving weak dependence of ER on Ri for $Ri \sim 1$

The major question arising from this paper concerns the interpretation and application of the results to steady flows, and to flows at very high Reynolds numbers (for a general discussion see Hunt & Carruthers 1990). The nonlinear dynamics of turbulence eddies in fact have a finite 'life-time' $T_L \sim L_X/u_3$ in unstratified turbulence, and of order α^{-1} in sheared turbulence ($Ri \leqslant 1$) (Kaltenbach *et al.* 1996) and N^{-1} in stratified turbulence ($Ri \geqslant 1$). When the results, e.g. for PE/VKE, have a steady asymptote, they may be applied in steady flows. But where the gross features of the turbulence are predicted to be unsteady (e.g. the formation of countergradient fluxes after $t \geqslant N^{-1}$), we might not expect to observe such fluxes in steady flows. Measurements in the atmospheric boundary layer when $Ri \sim 0.25$ (and $Nt \to \infty$) do not exhibit countergradient effects in statistically steady conditions. But they tend to be clearly observed during unsteady intermittent events.

Turbulent shear flows can only be steady when the mean velocity gradient is non-uniform, because then the vorticity dynamics inhibit the 'growth' of large-length-scale eddies (e.g. Hunt & Morrison 2000). However, we conclude that the mechanism for the 'suppression' of turbulence is local and is likely to be dominated by changes to the generation mechanism, independent of large-scale non-uniformities. This mechanism is not related to the suppression of any inviscid instability, which depends on the form of the large-scale mean velocity profile. Another reason why this local mechanism for Ri_{crit} is a robust concept comes from a simple Lagrangian analysis of finite-sized spherical fluid particles oscillating in a uniform shear flow. By combining the analysis of Pearson *et al.* (1983), and Auton, Hunt & Prud'homme (1988), it is found that the increasing shear stress associated with the particles' motion is suppressed for $Ri > Ri_{crit}$, where $Ri_{crit} \sim 1/4$.

Another unresolved problem is the Pr-dependence of the energy ratio ER and the countergradient flux. Although the results of RDT for $Pr = 1$ showed high-wavenumber countergradient flux consistent with the experiments, the experiments for stratified shear flow show the same results irrespective of Pr, while with no shear, wind tunnel experiments ($Pr = 0.7 < 1$) show a low-wavenumber countergradient flux. The energy ratio ER will also depend on Pr, as the viscosity affects VKE and PE differently (figures 4, 5).

In the atmosphere and the ocean, anisotropic initial conditions are often more relevant (Gargett 1988). For example, Gargett, Merryfield & Holloway (2003) used anisotropic initial conditions to investigate the double-diffusion processes in the ocean for relatively weak stratification ($Fr > 1$). The RDT solutions for initially anisotropic stratified rotating turbulence without mean shear have been considered by Hanazaki (2002), but similar effects on the shear flow still need to be assessed.

We finally note that a more complete applicability condition of RDT than described in § 2 would be established by also considering the energy ratio of the vortex mode to the wave mode, for example using the Craya–Herring frame (Godeferd & Cambon 1994). Such an estimate would be possible by calculating the initial ratio of the vortex-mode energy to the wave-mode energy. We note that DNS with no initial vortex energy shows very small vortex-mode energy even at large times (Métáis & Herring 1989). However, in shear flow there is both linear and nonlinear energy exchange between these two modes and with the potential energy. Thus we still need to determine what proportion of the vortex-mode component is related to the nonlinear motion in the subsequent time development.

The authors would like to thank Dr J. Iino of Tohoku University for numerical evaluation of the Reynolds stress shown in figure 3. J.C.R.H. acknowledges support from the Natural Environment Research Council to the Centre for Polar Observation and Modelling of University College London.

REFERENCES

Auton, T. R., Hunt, J. C. R. & Prud'homme, M. 1988 The force exerted on a body in inviscid unsteady non-uniform rotational flow. *J. Fluid Mech.* **197**, 241–257.

Batchelor, G. K. 1953 *The Theory of Homogeneous Turbulence*. Cambridge University Press.

Batchelor, G. K. & Proudman, I. 1954 The effect of rapid distortion of a fluid in turbulent motion. *Q. J. Mech. Appl. Maths* **7**, 83–103.

Britter, R. E., Hunt, J. C. R., Marsh, G. L. & Snyder, W. H. 1983 The effects of stable stratification on turbulent diffusion and the decay of grid turbulence. *J. Fluid Mech.* **127**, 27–44.

Cambon, C. 2002 Dynamics of rotating stably stratified flows. In *Statistical Theories and Computational Approaches to Turbulence* (ed. Y. Kaneda & T. Gotoh). pp. 25–59, Springer.

Craft, T. J., Ince, N. Z. & Launder, B. E. 1996 Recent developments in second-moment closure for buoyancy-affected flows. *Dyn. Atmos. Oceans* **23**, 99–114.

Csanady, G. T. 1964 Turbulent diffusion in a stratified fluid. *J. Atmos Sci.* **21**, 439–447.

Derbyshire, S. H. 1994 A 'balanced' approach to stable boundary layer dynamics. *J. Atmos. Sci.* **51**, 3486–3504.

Derbyshire, S. H. & Hunt, J. C. R. 1993 Structure of turbulence in stably stratified atmospheric boundary layers; Comparison of large eddy simulations and theoretical results. In *Waves and Turbulence in Stably Stratified Flows* (ed. S. D. Mobbs & J. C. King), pp. 23–59, Clarendon Press.

Fernando, H. J. S. & Hunt, J. C. R. 1996 Some aspects of turbulence and mixing in stably stratified layers. *Dyn. Atmos. Oceans* **23**, 35–62.

Galmiche, M. & Hunt, J. C. R. 2002 The formation of shear and density layers in stratified turbulent flows: linear processes. *J. Fluid Mech.* **455**, 243–262.

Gargett, A. E. 1986 Small-scale parameterization in large-scale ocean models. In *Advanced Physical Oceanographic Numerical Modelling*. NATO ASI Series C, vol. 186 (ed. J. J. O'Brien & D. Reidel), p. 10. Kluwer.

Gargett, A. E. 1988 The scaling of turbulence in the presence of stable stratification. *J. Geophys. Res.* **93** (C5), 5021–5036.

Gargett, A. E., Merryfield, W. J. & Holloway, G. 2003 Direct numerical simulation of differential scalar diffusion in three-dimensional stratified turbulence. *J. Phys. Oceanogr.* **33**, 1758–1782.

Gerz, T. & Schumann, U. 1991 Direct simulation of homogeneous turbulence and gravity waves in sheared and unsheared stratified flows, In *Turbulent Shear Flows 7*, pp. 27–45. Springer.

Gerz, T., Schumann, U. & Elghobashi, S. E. 1989 Direct numerical simulation of stratified homogeneous turbulent shear flows. *J. Fluid Mech.* **200**, 563–594.

Gerz, T. & Yamazaki, H. 1993 Direct numerical simulation of buoyancy-driven turbulence in stably stratified fluid. *J. Fluid Mech.* **249**, 415–440.

Gibson, C. H. & Schwarz, W. H. 1963 The universal equilibrium spectra of turbulent velocity and scalar fields. *J. Fluid Mech.* **16**, 365–384.

Godeferd, F. S. & Cambon, C. 1994 Detailed investigation of energy transfers in homogeneous stratified turbulence. *Phys. Fluids* **6**, 2084–2100.

Hanazaki, H. 2002 Linear processes in stably and unstably stratified rotating turbulence. *J. Fluid Mech.* **465**, 157–190.

Hanazaki, H. & Hunt, J. C. R. 1996 Linear processes in unsteady stably stratified turbulence. *J. Fluid Mech.* **318**, 303–337.

Hanazaki, H. & Hunt, J. C. R. 1999 Linear processes in unsteady stably stratified turbulence with mean shear. In *Turbulence Structure and Vortex Dynamics, Isaac Newton Institute Programme on Turbulence*.

Hanazaki, H. & Hunt, J. C. R. 2001 Linear processes in unsteady stratified sheared turbulence. In *Proc. IUTAM Symp. on Geometry and Statistics of Turbulence, Hayama, Japan, November 1–5, 1999* (ed. T. Kambe, T. Nakano & T. Miyauchi), pp. 291–296. Kluwer.

Herring, J. R. & Métais, O. 1989 Numerical experiments in forced stably stratified turbulence. *J. Fluid Mech.* **202**, 97–115.

Holmes, P., Lumley, J. L. & Berkooz, G. 1996 *Turbulence, Coherent Structures, Dynamical Systems and Symmetry*. Cambridge University Press.

Holt, S. E., Koseff, J. R. & Ferziger, J. H. 1992 A numerical study of the evolution and structure of homogeneous stably stratified turbulence. *J. Fluid Mech.* **237**, 499–539.

Hunt, J. C. R. & Carlotti, P. 2001 Statistical structure at the wall of the high Reynolds number turbulent boundary layer. *Flow Turbulence Combust.* **66**, 453–475.

Hunt, J. C. R. & Carruthers, D. J. 1990 Rapid distortion theory and the 'problems' of turbulence. *J. Fluid Mech.* **212**, 497–532.

Hunt, J. C. R., Kaimal, J. C. & Gaynor, J. E. 1985 Some observations of turbulence structure in stable layers. *Q. J. R. Met. Soc.* **111**, 793–815.

Hunt, J. C. R. & Morrison, J. F. 2000 Eddy structure in turbulent boundary layers. *Eur. J. Mech.* B – *Fluids* **19**, 673–694.

Hunt, J. C. R., Sandham, N. D., Vassilicos, J. C., Launder, B. E., Monkewitz, P. A. & Hewitt, G. F. 2001 Developments in turbulence research: a review based on the 1999 Programme of the Isaac Newton Institute, Cambridge. *J. Fluid Mech.* **436**, 353–391.

Hunt, J. C. R., Stretch, D. D. & Britter, R. E. 1988 Length scales in stably stratified turbulent flows and their use in turbulence models. In *Stably Stratified Flow and Dense Gas Dispersion* (ed. J. S. Puttock), pp. 285–321. Clarendon.

Ince, E. L. *Ordinary Differential Equations*. Dover.

Itsweire, E. C., Helland, K. N. & Van Atta, C. W. 1986 The evolution of grid-generated turbulence in a stably stratified fluid. *J. Fluid Mech.* **162**, 299–338.

Jacobitz, F. G., Sarkar, S. & Van Atta, C. W. 1997 Direct numerical simulation of the turbulence evolution in a uniformly sheared and stably stratified flow. *J. Fluid Mech.* **342**, 231–261.

Kaltenbach, H. -J., Gerz, T. & Schumann, U. 1994 Large eddy simulation of homogeneous turbulence and diffusion in stably stratified shear flow. *J. Fluid Mech.* **280**, 1–40.

Kaneda, Y. 2000 Single-particle diffusion in strongly stratified and/or rapidly rotating turbulence. *J. Phys. Soc. Japan* **69**, 3847–3852.

Kaneda, Y. & Ishida, T. 2000 Suppression of vertical diffusion in strongly stratified turbulence. *J. Fluid Mech.* **402**, 311–327.

Keller, K. H. & Van Atta, C. W. 2000 An experimental investigation of the vertical temperature structure of homogeneous stratified shear turbulence. *J. Fluid Mech.* **425**, 1–29.

Kevlahan, N. K.-R. & Hunt, J. C. R. 1997 Nonlinear interactions in turbulence with strong irrotational straining. *J. Fluid Mech.* **337**, 333–364.

Kimura, Y. & Herring, J. R. 1996 Diffusion in stably stratified turbulence. *J. Fluid Mech.* **328**, 253–269.

Komori, S. & Nagata, K. 1996 Effects of molecular diffusivities on counter-gradient scalar and momentum transfer in strong stable stratification. *J. Fluid Mech.* **326**, 205–237.

Komori, S., Ueda, H., Ogino, F. & Mizushina, T. 1983 Turbulence structure in stably stratified open-channel flow. *J. Fluid Mech.* **130**, 13–26.

Lee, M. J., Kim, J. & Moin, P. 1990 Structure of turbulence at high shear rate. *J. Fluid Mech.* **216**, 561–583.

Lienhard, J. H. & Van Atta, C. W. 1990 The decay of turbulence in thermally stratified flow. *J. Fluid Mech.* **210**, 57–112.

Métais, O. & Herring, J. 1989 Numerical simulations of freely evolving turbulence in stably stratified fluids. *J. Fluid Mech.* **202**, 117–148.

Miles, J. W. 1961 On the stability of heterogeneous shear flow. *J. Fluid Mech.* **10**, 496–508.

Moffatt, H. K. 1967 The interaction of turbulence with strong wind shear. In *Proc. URSI-IUGG Intl Colloquium on Atmospheric Turbulence and Radio Wave Propagation Moscow, June 15–22, 1965* (ed. A. M. Yaglom & V. I. Tatarsky), pp. 139–154. Nauka, Moscow.

Monti, P., Fernando, H. J. S., Princevac, M., Chan, W. C., Kowalewski, T. A. & Pardyjak, E. R. 2002 Observation of flow and turbulence in the nocturnal boundary layer over a slope. *J. Atmos. Sci.* **59**, 2513–2534.

Pearson, H. J. & Linden, P. F. 1983 The final stage of decay of turbulence in stably stratified fluid. *J. Fluid Mech.* **134**, 195–203.

Pearson, H. J., Puttock, J. S. & Hunt, J. C. R. 1983 A statistical model of fluid-element motions and vertical diffusion in a homogeneous stratified turbulent flow. *J. Fluid Mech.* **129**, 219–249.

Piccirillo, P. & Van Atta, C. W. 1997 The evolution of a uniformly sheared thermally stratified turbulent flow. *J. Fluid Mech.* **334**, 61–86.

Ramsden, D. & Holloway, G. 1992 Energy transfers across an internal wave-vortical mode spectrum. *J. Geophys. Res.* **97** (C3), 3659–3668.

Richardson, L. F. 1926 Atmospheric diffusion shown on a distance-neighbour graph. *Proc. R. Soc. Lond.* A **110**, 709–737.

Riley, J. J. & Lelong, M. P. 2000 Fluid motions in the presence of strong stable stratification. *Annu. Rev. Fluid Mech.* **32**, 613–657.

Riley, J. J., Metcalfe, R. W. & Weissman, M. A. 1981 Direct numerical simulations of homogeneous turbulence in density stratified fluids. *Nonlinear Properties of Internal Waves. AIP Conference Proc.* vol. 76, pp. 79–112. American Institute of Physics.

Rogers, M. M. 1991 The structure of a passive scalar field with a uniform mean gradient in rapidly sheared homogeneous turbulent flow. *Phys. Fluids* A **3**, 144–154.

Rohr, J. J., Itsweire, E. C., Helland, K. N. & Van Atta, C. W. 1988 Growth and decay of turbulence in a stably stratified shear flow. *J. Fluid Mech.* **195**, 77–111.

Saffman, P. G. 1967 The large-scale structure of homogeneous turbulence. *J. Fluid Mech.* **27**, 581–593.

Salhi, A. 2002 Similarities between rotation and stratification effects on homogeneous shear flow. *Theor. Comput. Fluid Dyn.* **15**, 339–358.

Salhi, A. & Cambon, C. 1997 An analysis of rotating shear flow using linear theory and DNS and LES results. *J. Fluid Mech.* **347**, 171–195.

Sawford, B. L. & Hunt, J. C. R. 1986 Effects of turbulence structure, molecular diffusion and source size on scalar fluctuations in homogeneous turbulence. *J. Fluid Mech.* **165**, 373–400.

Schumann, U. 1996 Direct and large eddy simulations of stratified homogeneous shear flows. *Dyn. Atmos. Oceans* **23**, 81–98.

Schumann, U. & Gerz, T. 1995 Turbulent mixing in stably stratified shear flows. *J. Appl. Met.* **34**, 33–48.

Stretch, D. D. 1986 The dispersion of slightly dense contaminations in a turbulent boundary layer. PhD Thesis, Dept. of Engineering, University of Cambridge.

Taylor, G. I. 1921 Diffusion by continuous movements. *Proc. Lond. Math. Soc.* (2), **20**, 196–212.

Taylor, G. I. 1931 Effect of variation in density on the stability of superposed streams of fluid. *Proc. R. Soc. Lond.* A **132**, 499–523.

Townsend, A. A. 1976 *The Structure of Turbulent Shear Flow*. Cambridge University Press.

Yoon, K. & Warhaft, Z. 1990 The evolution of grid generated turbulence under conditions of stable thermal stratification. *J. Fluid Mech.* **215**, 601–638.